Clay Minerals (1997) **32**, 153–179

Isomorphous cation distribution in celadonites, glauconites and Fe-illites determined by infrared, Mössbauer and EXAFS spectroscopies

V. A. DRITS, L. G. DAINYAK, F. MULLER*, G. BESSON* AND A. MANCEAU†

*Geological Institute of the Russian Academy of Sciences, Pyzhevsky per.7, Moscow, Russia, *CRMD, University of Orléans - CNRS, BP 6759, 45067 Orléans, Cedex 2, France, and † Environmental Geochemistry Group, LGIT, IRIGM, University of Grenoble, BP 53, 38041 Grenoble, France*

(*Received 26 March 1996; revised 7 August 1996*)

ABSTRACT: Celadonite, glauconite and Fe-illite samples were studied by XRD, EXAFS, IR and Mössbauer spectroscopy. The samples were monomineralic and corresponded to 1*M* polytype. In the OH-stretching region of the IR spectra the content of each definite pair of cations bonded to OH groups was determined. The number of heavy (Fe) and light (Al, Mg) octahedral cations nearest to Fe was found by the EXAFS technique. The predicted quadrupole splitting values for each definite arrangement of cations nearest to Fe^{3+} were used to interpret the Mössbauer spectra. After the fitting procedure, the intensity of each doublet corresponded to a definite set of local cation arrangements around Fe^{3+} and to a definite occurrence probability of these arrangements. Computer simulation and the experimental data obtained were used to reconstruct the distribution of isomorphous octahedral cations in the 2:1 layers. For all samples, R^{2+} cations prefer to occupy one of the two symmetrically independent *cis*-sites and R^{2+}-R^{2+} and/or Al-Fe^{3+} were prohibited in the directions forming $\pm 120^{\circ}$ with the *b* axis. Therefore, octahedral sheets of the samples revealed domain structure, in which domains differ in size, in the nature of predominant cation and/or by cation ordering.

One of the characteristic features of phyllosilicates and, in particular, dioctahedral micas, is a wide variation of chemical compositions. Different samples of the same mineral may differ not only in octahedral and tetrahedral cation contents of 2:1 layers, but also in their long- and short-range ordering in isomorphous cation distribution. Determination of the actual cation distribution in dioctahedral micas is a complex problem. X-ray diffraction (XRD) yields data only on the averaged composition of cations in the unit-cell sites, ignoring a possible short-range ordering. For finely dispersed minerals containing stacking faults, even this information is often difficult to obtain.

Spectroscopic methods are, therefore, especially useful, since they probe local atomic environments and have a potential to determine short-range cation ordering. Utilization of spectroscopic methods, however, often meets certain difficulties. One of the main problems is that most of these methods are indirect, that is, they provide indirect structural information about a sample under study. For this reason, interpretation of spectroscopic data is not always feasible or properly based.

One of the effective ways to determine the actual cation distribution consists of the application of complex diffraction and spectroscopic methods to the same sample. Obviously, the greater the number of methods involved, the more comprehensive the structural information obtained. Each method, however, has its own advantages and limitations and therefore provides only a partial solution to a

general problem of cation order/disorder in dioctahedral mica structures. Therefore, even if unambiguous interpretation of experimental data is provided, the actual cation distribution pattern can hardly be achieved even using a combination of various diffraction and spectroscopic methods.

The solution to this problem proposed by Dainyak *et al*. (1992) was based on computer simulation of the two-dimensional distribution of octahedral cations in dioctahedral 2:1 layer silicates. Using the experimental data obtained by different methods, this simulation can reconstruct the actual cation distribution in dioctahedral mica structures. In fact, this approach can be considered as a 'bridge' between data obtained by different methods as well as between short-range and long-range cation order.

In this paper, computer simulation was used to reconstruct a two-dimensional cation distribution in celadonite, glauconite and Fe-illite samples using the experimental data obtained by XRD, X-ray absorption fine structure (EXAFS) analysis, infrared (IR) and Mössbauer spectroscopies.

DETERMINATION OF THE OCTAHEDRAL CATION DISTRIBUTION IN DIOCTAHEDRAL MICAS BY DIFFRACTION AND SPECTROSCOPIC METHODS

X-ray diffraction

This method allows us to determine the average occupancies of *trans*- and *cis*-sites in mica unit-cells. Traditionally, most researchers believed that all illites consist of 2:1 layers with *trans*-vacant octahedra. This assumption was based on single crystal X-ray structure refinements by which octahedral cations in 2:1 layers of various polytypes of muscovite, paragonite and margarite were shown to occupy only *cis*-sites (Bailey, 1984). On the other hand, until recently it was assumed that in celadonite, glauconite and nontronite structures, both *cis*- and *trans*-octahedra can be occupied by Fe^{3+} (Heller-Kallai & Rozenson, 1981; De Grave *et al*., 1985; Johnston & Cardile, 1987; Cardile & Brown, 1988).

Drits *et al*. (1984a) formulated structural and diffraction criteria to distinguish between dioctahedral 1*M* micas consisting of *cis*-vacant (cv 1*M*) or *trans*-vacant (tv 1*M*) 2:1 layers. Based on these criteria, cv 1*M* illites were found in different geological environments (Zvyagin *et al*., 1985; Drits *et al*., 1993a; Reynolds & Thompson, 1993). Conversely, Sakharov *et al*., (1990) and Drits *et al*. (1993b) studied a large collection of glauconites differing in chemical composition, age, location and structural perfection. They found that all glauconites belonging to the tv 1*M* polytype confirmed the conclusion that the structure of Fe^{3+}-rich dioctahedral 2:1 layer silicates consists of tv layers (Besson *et al*., 1983; Tsipursky & Drits, 1984; Dainyak *et al*., 1984b, 1984c; Tsipursky *et al*., 1978, 1985).

Nevertheless, in order to obtain experimental data on occupancies of *cis*- and *trans*-sites within the unit-cell, the diffraction characteristics of cv 1*M* and tv 1*M* structural varieties were compared with those observed experimentally for the studied samples. Two basic criteria permit us to distinguish between the stuctural polymorphs: first, XRD patterns of tv 1*M* micas contain strong $11\bar{1}$, $11\bar{2}$ and 112 reflections, while the 111 reflection has zero intensity; conversely, XRD patterns of cv 1*M* micas have 111, $11\bar{2}$, 112 and $11\bar{3}$ reflections with similar intensities; second, the values of I *c*cosß/*a* I, which characterize relative displacements of two adjacent layers with respect to each other along the *a*-axis, are distinctly >1/3 for tv 1*M* and distinctly less than this value for cv 1*M* polymorphs. Here *a*, *c* and ß are unit-cell parameters.

IR spectroscopy

The characteristic feature of dioctahedral mica IR spectra in the OH-stretching region is that each definite type of cation bonded to an OH group is determined by a definite position of the corresponding OH band, whereas the content of a definite cationic pair is determined by the integrated optical density, i.e. the area of the corresponding OH band is transformed to the optical density. Slonimskaya *et al*. (1986) were the first to work out the approach of determining quantitatively the content of octahedral cationic pairs bonded to OH groups, as well as the content of octahedral cations in the mica unit-cell. Besson & Drits (1997a, b) improved the approach of Slonimskaya *et al*. (1986). They revised the relationships between the types of cations bonded to OH groups and the corresponding OH-stretching frequencies. At present, the quantitative analysis of the dioctahedral mica IR spectra can be successfully applied for the study of cation short-range ordering.

Unfortunately, this technique provides information on cation distribution at a one-dimensional level only, i.e. for only one crystallographic direction (Besson *et al*., 1987).

Computer simulation of cation distribution using IR data. Dainyak *et al*. (1992) elaborated a computer program in order to distribute four types of cations: Mg, Fe^{2+}, Fe^{3+} and Al within a *trans*-vacant octahedral sheet. As basic global parameters of the octahedral cation distribution, the occurrence probabilities W_{ij} (i, j = Mg, Fe^{2+}, Fe^{3+}, Al) for cations of the i and j types bonded to OH groups were used. These values characterize the cation distribution between adjacent *cis*-octahedra in a fixed direction. In 1*M* dioctahedral micas, this direction coincides with the *b* axis. The IR quantitative analysis yields integrated optical densities that are proportional to the symmetric sums of occurrence probabilities $W_{ij} + W_{ji}$. Thus, to define a real occurence probability, one has to determine, for every cation, the degree of its preference to one of the *cis*-sites, I or II (Fig. 1). For example, Table 1 contains the IR spectrum decomposition for the Z1 sample represented as W_{ij} sets for two limiting cases: (1) *cis*-sites I and II are equivalent with respect to different cation types (referred to as 'equiv'); and (2) R^{2+} cations prefer to occupy one of the two possible *cis*-sites (referred to as 'pref'). Even one of these conditions alone admits a huge number of possible cation distributions with the same set of integrated optical densities.

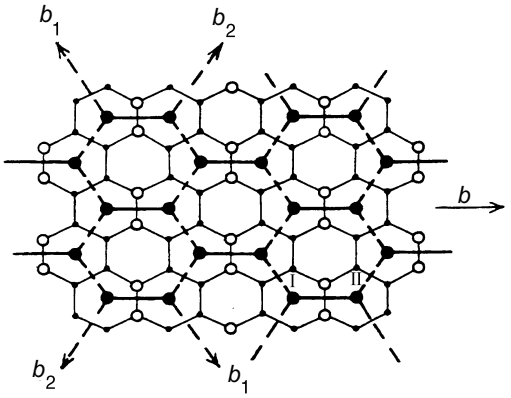

FIG. 1. Honeycomb pattern of the dioctahedral sheet. Solid and dashed lines connecting cations correspond to the *b* axis and b_1, b_2 directions respectively. Open and black large circles correspond, respectively, to OH groups and octahedral cations occcupying *cis*-sites.

Cation pairs may be distributed among the sites available at random (referred to as 'cons'), and then two types of limitations can be introduced either separately or simultaneously. One of these limitations leads to a distribution with prohibition of R^{2+}-R^{2+} pairs along the b_1 and b_2 directions running at $\pm 120^\circ$ or $\pm 60^\circ$ with respect to the *b*-direction (Fig. 1). Such a limitation should imply that octahedral cation distribution obeys the Pauling rule or the principle of homogeneous charge distribution (HCD), that is, the compensation of the negative charge is approximately the same for each anion. The other limitation provides a prohibition against Fe^{3+}-Al pairs along the b_1 and b_2 directions. Its application promotes the segregation of Al and Fe^{3+}. The cation distribution with the minimum values for N_{22} and/or N_{FA} corresponding to the number of R^{2+}-R^{2+} and Fe^{3+}-Al pairs, respectively, is accomplished by a penalty function, $f(\alpha) = \alpha N_{FA} + (1-\alpha)N_{22}$, where the α parameter is to be pre-set. Dainyak *et al*. (1992) showed that three values of α have a practical meaning: if α is zero, pairs R^{2+}-R^{2+} should be forbidden in b_1 or b_2 directions, $\alpha = 1$ implies prohibition of Fe^{3+}-Al pairs in these directions, and both limitations take place at $\alpha = 0.5$.

TABLE 1. Probability parameters W_{ij} (i, j = Mg, Fe^{2+}, Fe^{3+}, Al) for Z1 sample when *cis*-sites are equivalent to different cation types ('equiv') and when R^{2+} cations prefer to occupy one of the two possible *cis*-sites ('pref').

Cationic pairs (ij)	W_{ij} 'equiv'	W_{ij} 'pref'
Fe^{3+} Fe^{3+}	0.137	0.137
Fe^{2+} Fe^{3+}	0.052	0.104
Al Fe^{3+}	0.013	0.013
Mg Fe^{3+}	0.281	0.561
Fe^{3+} Fe^{2+}	0.052	–
Fe^{2+} Fe^{2+}	0.066	0.066
Al Fe^{2+}	–	–
Mg Fe^{2+}	0.018	0.018
Fe^{3+} Al	0.013	0.013
Fe^{2+} Al	–	–
Al Al	0.007	0.007
Mg Al	0.013	0.025
Fe^{3+} Mg	0.280	–
Fe^{2+} Mg	0.018	0.018
Al Mg	0.012	–
Mg Mg	0.038	0.038

For each cation distribution, the following parameters are determined: relative weights of each local cation environment around Fe^{3+} consisting of three octahedral cations nearest central Fe^{3+}, i.e. W(3Al), W(2AlFe^{3+}), W(3Mg), etc.; average numbers of 'light' (Al, Mg) and 'heavy' (Fe) cations nearest to Fe-cations, average numbers of Al-Al, Fe-Fe, Mg-Mg pairs, etc.

EXAFS

This technique is a local structural probe. It provides quantitative structural information, which in this case is restricted to the three or four nearest atomic shells surrounding the X-ray absorber. For each shell, the identity and number of atomic neighbours and interatomic distances may be obtained by quantitative spectral analysis. Similarly to diffraction techniques, scattering amplitude functions vary smoothly with atomic numbers, precluding the discrimination between Mg and Al, on the one hand, and Mn, Fe, Ni..., on the other hand, among cation neighbours. Application of EXAFS to the distribution of cations in mineral structures requires good precision in the determination of coordination numbers (N), which seldom exceeds 10−20% regardless of the compound (Teo, 1986). In clay minerals, however, this precision is markedly better than 20% due to the fact that (1) electronic waves backscattered by Mg, Al and 3d atoms are precisely out of phase over most of the wavevector span (provided these atoms are at the same distance from the central atom), and (2) the total number of nearest cations can generally be obtained from other techniques. For instance, by confronting EXAFS and NMR results obtained on the same suite of mica samples, Manceau *et al*. (1990) showed that the relative precision on N was better than 10%.

Another difficulty faced with the quantitative analysis of EXAFS spectra in phyllosilicate structures concerns the contribution of the tetrahedral cations. The contributions to EXAFS of the successive atomic shells surrounding the X-ray absorber are generally filtered by Fourier transforms. In 2:1 phyllosilicates, octahedral cations share six edges with neighbouring octahedra at ∼3.0−3.1 Å, and four corners with Si tetrahedra at ∼3.2−3.3 Å. The closeness of octahedral and tetrahedral shells prevents their separation by Fourier transforms, and the contribution of the latter needs to be added when fitting Fourier filtered EXAFS data.

In the present study, the strategy adopted to fit the EXAFS data was particularly stringent in order to obtain confidence in structural parameters and, specifically, in coordination numbers $N_{Fe\text{-}Fe}$, $N_{Fe\text{-}(Mg,Al)}$. The variation range of refined structural parameters was either restricted or fixed on the basis of independent structural information obtained from the other techniques. (1) The total number of octahedral cations nearest to Fe was fixed as three. This value follows from the chemical composition and the *trans*-sites being vacant. (2) In clay mineral structures, the distances between nearest octahedral cations is equal to b/3. This value was determined with high precision by XRD for each sample. (3) Application of the technique developed by Smoliar-Zviagina (1993) for determination of interatomic distances in glauconite structures has shown that, regardless of chemical composition, the distance between Fe and (Si, Al) cations is between 3.22 Å and 3.24 Å. Given that the precision of EXAFS on interatomic distances is not better than a few hundredths of 1 Å, this distance was assumed as 3.23 Å for all samples.

Mössbauer spectroscopy

Until recently, the widely accepted interpretation of Mössbauer spectra of Fe^{3+}-rich dioctahedral 2:1 layer silicates consisted of decomposition of the corresponding spectrum into two main doublets which were assumed to be related to Fe^{3+} ions in *cis*- and *trans*-octahedra of 2:1 layers (Heller-Kallai & Rozenson, 1981; Rozenson & Heller-Kallai, 1978; Govaert *et al*., 1978; Kotlicki *et al*., 1981; De Grave *et al*., 1985; Johnston & Cardile, 1987; Cardile & Brown, 1988). As was mentioned, the XRD data showed that *trans*-sites are vacant in most Fe^{3+}-rich dioctahedral 2:1 layer silicates. For this reason, the conventional interpretation of Mössbauer spectra of these minerals had to be reconsidered. However, the poor resolution of Mössbauer spectra of celadonites and glauconites leads to many problems in their interpretation. First of all, there is an uncertainty in the number of doublets fitted and in parameters that should be used for their characterization. For this reason, statistically good fits may be achieved with various numbers of doublets and/or their parameters. But even if the number of doublets is found correctly, the problem of structural identification of these doublets will remain.

Recent Mössbauer study of trioctahedral micas (Hargraves *et al*., 1990; Rancourt, 1994) and illites

(Murad & Wagner, 1994) has shown that the octahedral Fe *cis*- and *trans*-sites cannot be resolved.

A new approach to the Mössbauer spectra interpretation consistent with diffraction data was developed by Bookin *et al*. (1978), Dainyak *et al*. (1981, 1984a,b,c, 1992) and Dainyak & Drits (1987). These authors showed that it is incorrect to assign Mössbauer doublets to model sites in the average unit-cell, in particular to *cis*- and *trans*-sites in the unit-cells of 2:1 layer silicates. In terms of their models, the observed difference of the quadrupole splittings of Fe^{3+} is caused by a distortion of the Fe^{3+}-octahedron due to the different local structural and chemical environments. The validity of the model was supported by calculations of the electric field gradients.

In micas with complex isomorphism, a wide variety of local cation environments near Fe^{3+} may take place. It is obvious that several cation arrangements should correspond to each Fe^{3+} doublet even if a number of the doublets is equal to four, for example. To solve this problem, an empirical relationship between the quadrupole splitting values, Δ, and the nature of the nearest cation neighbours was used

$$\Delta(\text{mm/s}) = 0.74 - 6.9(d^{av} - 1.93)^{0.83} + (3 - Z^{av})^{0.15} \quad (1)$$

where d^{av} is the bond length averaged over the cation-anion bond lengths in the three octahedra nearest to the Fe^{3+}-octahedron, bearing in mind that $d_{Fe^{3+}}$ = 1.98 Å, $d_{Fe^{2+}}$ = 2.12 Å, d_{Mg} = 2.07 Å and d_{Al} = 1.93 Å; Z^{av} is the cation charge averaged over three cations nearest to Fe^{3+}. The second and third terms of this equation reflect the influence of the heterogenity of sizes and charges of cations surrounding Fe^{3+}, respectively, on the electric field gradient on Fe^{3+}.

Equation (1) yields 0.74 and 0.17 mm/s for the arrangements 3Al and $3Fe^{3+}$, respectively. The quoted Δ values are observed in Mössbauer spectra of muscovite and ferripyrophyllite (Dainyak & Drits, 1987), and their assignments are unambiguous. The derivation of this equation will be considered by Dainyak & Drits (in prep.).

Table 2 contains Δ values calculated for all possible cation arrangements around Fe^{3+}. Each specific cation distribution contains a definite proportion of each type of local cation configuration around Fe^{3+}. It is assumed that the statistically weighted sum of close quadrupole splitting values corresponding to a definite group of the local cation arrangements should be equal or close to a value of quadrupole doublet in the Mössbauer spectrum of a sample under study. Therefore, an analysed cation distribution can be considered as corresponding to the actual one if all types of cation combinations can be grouped in accordance with the number of decomposed Fe^{3+} doublets so that the statistically weighted sum of quadrupole splittings within each group corresponds to one of the observed quadrupole doublets. Therefore, in this work, we use the method which includes a 'hard' model with an *a priori* known quadrupole splitting for each definite local cation environment around Fe^{3+}.

TABLE 2. Quadrupole splitting values Δ calculated for all possible local cation arrangements around Fe^{3+} using relationship (1).

Local arrangement	Δ(mm/s)	Local arrangement	Δ(mm/s)
$3R^{2+}$	0.00	$2MgFe^{3+}$	0.58
$3R^{3+}$	0.17	$Fe^{2+}2Fe^{3+}$	0.59
$2Fe^{2+}Mg$	0.13	$AlMgFe^{2+}$	0.58
$2MgFe^{2+}$	0.26	$AlFe^{2+}Fe^{3+}$	0.74
$2Fe^{2+}Fe^{3+}$	0.31	2MgAl	0.72
$2Fe^{3+}Al$	0.33	$2Fe^{3+}Mg$	0.74
3Mg	0.39	3Al	0.74
$2Fe^{2+}Al$	0.44	$AlMgFe^{3+}$	0.89
$MgFe^{2+}Fe^{3+}$	0.44	$2AlFe^{2+}$	0.89
$2AlFe^{3+}$	0.51	2AlMg	1.05

SAMPLES

A collection of monomineral celadonite, globular glauconite and Fe-illite samples differing in chemical composition was analysed. The structural formulae of the samples as well as the references with their mineralogical description are given in Table 3.

EXPERIMENTAL

XRD data

The main purpose of the XRD experiments was to check a monomineral phase composition, to determine unit-cell parameters, and to obtain information on octahedral cation distribution over *trans*- and *cis*-sites within the unit-cells of the samples studied.

The XRD powder patterns were obtained using Mo-*K*α radiation with an INEL CPS 120 diffractometer supplied with a graphite monochromator and a curved position sensitive detector. This detector permits simultaneous recording of diffraction intensities in a wide interval of *d*-values. The sample holder was a thin tube made from Lindeman glass with a diameter of 1 mm.

IR data

The IR spectra in the OH-stretching region were obtained with a BRUKER - 113 spectrometer. The alkali halide pressed disk technique was used: 3 mg of samples of particle size <2 μm was added to ~200 mg of KBr in a steel capsule. Steel balls were added, and the mixture was ground and mixed for 2 min in a vibratory grinder. The disk obtained after pressing was heated at ~120°C for 12 h to remove most of the adsorbed water. Transmission intensities were recorded at 1 cm^{-1} intervals, and each spectrum contained nearly 1000 points. The transmitted intensity, *I*, for each frequency was transformed to optical density, *D*, according to the equation $D = \ln(Io/I)$, where *Io* is the intensity of the incident beam. The integrated optical densities are treated as occurrence probabilities, $(W_{ij} + W_{ji})$, for cations of the *i* and *j* types bonded to OH groups.

The decomposition of IR spectra of dioctahedral micas into individual OH bands was described by Slonimskaya *et al.* (1986) and by Besson & Drits (1996a). The computer program written by B. Lanson was used to extract up to 15 individual bands in the experimental spectrum between the wavenumbers from 3400cm^{-1} – 3800cm^{-1}. All OH

TABLE 3. Cation composition of samples studied calculated per $O_{10}(OH)_2$.

	Sample								
Cation	Z1	69	Pil	6869	402	CH	655	E8/2	BP
Si	3.96	3.94	3.73	3.78	3.83	3.42	3.71	3.65	3.46
Al^{IV}	0.04	0.06	0.27	0.22	0.17	0.58	0.24	0.35	0.54
Al	0.05	0.05	0.44	0.55	0.56	0.92	0.16	0.68	1.11
Fe^{3+}	0.96	1.15	0.93	0.89	0.58	0.74	1.10	0.79	0.41
Fe^{2+}	0.26	0.36	0.21	0.18	0.46	0.07	0.12	0.10	0.13
Mg	0.73	0.41	0.42	0.39	0.52	0.27	0.63	0.43	0.35
K	0.89	0.83	0.75	0.80	0.72	0.79	0.92	0.78	0.74
Na	–	0.01	0.06	–	0.07	0.02	–	0.01	0.01
Ca	0.10	0.03	0.05	–	0.01	0.05	0.05	0.09	0.06
Ref.	1	2	3	4	5	6	7	8	9

1: Celadonite (Malkova, 1956); 2: celadonite (Pavlishin *et al*., 1978);
3: glauconite (Drits *et al*., 1993b); 4: glauconite (Shutov *et al*., 1975);
5: celadonite (Ivanovskaya *et al*., 1989);
6: Fe-illite sample from Syria, Stratum alp, given by Dr Muraviev V.I. (GIN RAN, Moscow);
7: glauconite (Drits *et al*., 1993b); 8: glauconite (Drits *et al*., 1993b);
9: Fe-illite (Drits *et al*., 1993b).

bands were assumed to have a Lorentzian form, and band position, width at half height, and intensity were used as the variable parameters describing individual bands. The quality of the decomposition was estimated from the χ^2 values as well as by the common agreement of all parts of the experimental IR spectrum profile with those of the IR spectrum synthesized by summation of all extracted individual bands. In addition, the octahedral cation content determined by wet chemical analysis for each sample was compared with that determined by the quantitative analysis of the IR spectra according to the technique elaborated by Slonimskaya *et al.* (1986) and Besson & Drits (1997b).

EXAFS data

Measurements were performed at the LURE synchrotron radiation facility, on the EXAFS 4 station using the X-ray beam emitted by the DCI storage ring. Spectra were collected in transmission mode, at the Fe-*K* edge. The incident white beam was monochromatized with Si(311) double crystals. Harmonics were removed with two borosilicate glass mirrors (Sainctavit *et al.*, 1988).

X-ray absorption spectra were treated following a standard procedure (Teo, 1986). Some Fe-*K* edge EXAFS spectra were obtained from raw absorption spectra by normalization to the absorption jump. The kinetic energy of the photoelectron was converted into the modulus of the wavevector k to obtain the $\chi(k)$ function. This function is the summation of the elementary contributions to the EXAFS spectra of the very first atomic shells surrounding Fe. The atomic-pair correlation function, or radial distribution function (RDF), was obtained by Fourier transforming $\chi(k)$ spectra to real space using a Kaiser window (Manceau & Combes, 1988). The RDFs are not corrected for atomic pairs phase shift functions, and thus each peak is displaced by short distances, $\sim\Delta R \approx 0.3-0.4$ Å from its crystallographic position. Structural parameters, namely the nature of the nearest atoms, interatomic distances (R), and coordination number (N), characterizing the atomic environment of Fe atoms were extracted by singling out and Fourier back-transforming individual RDF peaks. This yields the contribution to the EXAFS spectrum of the atomic shell(s) attached to the selected RDF peak. This experimental Fourier filtered partial contribution to the EXAFS spectrum was then least-square fitted by a theoretical curve. The theoretical phase shift and amplitude function of McKale *et al.* (1988) were used to construct theoretical spectra. Sample 69 was used to test their correctness as its local structure was known from the other methods. The Γ parameter, which is related to the electron mean free path τ by the relation $\Gamma = k/\tau$ (Teo, 1986), was determined from this reference and then kept constant for the unknown samples. Figure 2a shows that a very good simulation of the experimental Fe-nearest cations contribution was obtained with the following parameters for the three nearest atomic shells: $N_{\text{Fe-Fe}} = 2.20$; $\sigma_{\text{Fe-Fe}} = 0.09$ Å; $R_{\text{Fe-Fe}} = 3.02$ Å; $N_{\text{Fe-(Mg,Al)}} = 0.80$; $\sigma_{\text{Fe-(Mg,Al)}} = 0.09$ Å; $R_{\text{Fe-(Mg,Al)}} = 3.02$ Å; $N_{\text{Fe-Si}} = 4$; $\sigma_{\text{Fe-Si}} = 0.07$ Å; $R_{\text{Fe-Si}} = 3.23$ Å; $\Delta E = 1.5$ eV; $\Gamma = 1.7$ Å^{-2}, where σ is the Debye-Waller term and ΔE a parameter needed to adjust the threshold energy. In this fit, only Γ and ΔE were allowed to vary without restriction: σ and N were constrained as follows: $0.07 \text{ Å} \leqslant \sigma \leqslant 0.10$ Å; $N_{\text{Fe-Fe}} + N_{\text{Fe-(Mg,Al)}} = 3.0$, and the other parameters were kept fixed. It should be emphasized that despite the very strong constraints of this fitting procedure, the quality of the fit is very good, which certifies the soundness of our strategy. In the fitting of the unknown samples, Γ, $N_{\text{Fe-Si}}$, $\sigma_{\text{Fe-Si}}$, and $R_{\text{Fe-Si}}$ were kept fixed to their previous values, $R_{\text{Fe-Fe}}$ and $R_{\text{Fe-(Mg,Al)}}$ were fixed to $b/3$, $R_{\text{Fe-Si}}$ to 3.23 Å and $N_{\text{Fe-Fe}} + N_{\text{Fe-(Mg,Al)}} = 3.0$; ΔE was allowed to vary and all σ values were constrained to $0.07 \text{ Å} \leqslant \sigma \leqslant 0.10$ Å.

Mössbauer spectra: data collection

The Mössbauer spectra of samples 655, Pil and BP were measured at room temperature using a ^{57}Co/Cr source and SM 2201 spectrometer. The velocity scale was calibrated with reference to α-Fe. To eliminate the orientation effects, the samples were prepared in a hollow cone form with an approximately 55° half-cone angle (Popov *et al.*, 1988). While a sample was in an inclined position, the absorber thickness did not exceed 7 mg Fe/cm^2. The Mössbauer spectrum of sample 68/69 was recorded at room temperature using a constant acceleration spectrometer with a ^{57}Co source in a rhodium matrix. This experiment was carried out by Dr D. Bonnin (Laboratoire de Physique Quantique de l'ESPCI, Paris). The experimental conditions for recording the Mössbauer spectrum of sample Z1 was described by Dainyak *et al.* (1984c). The

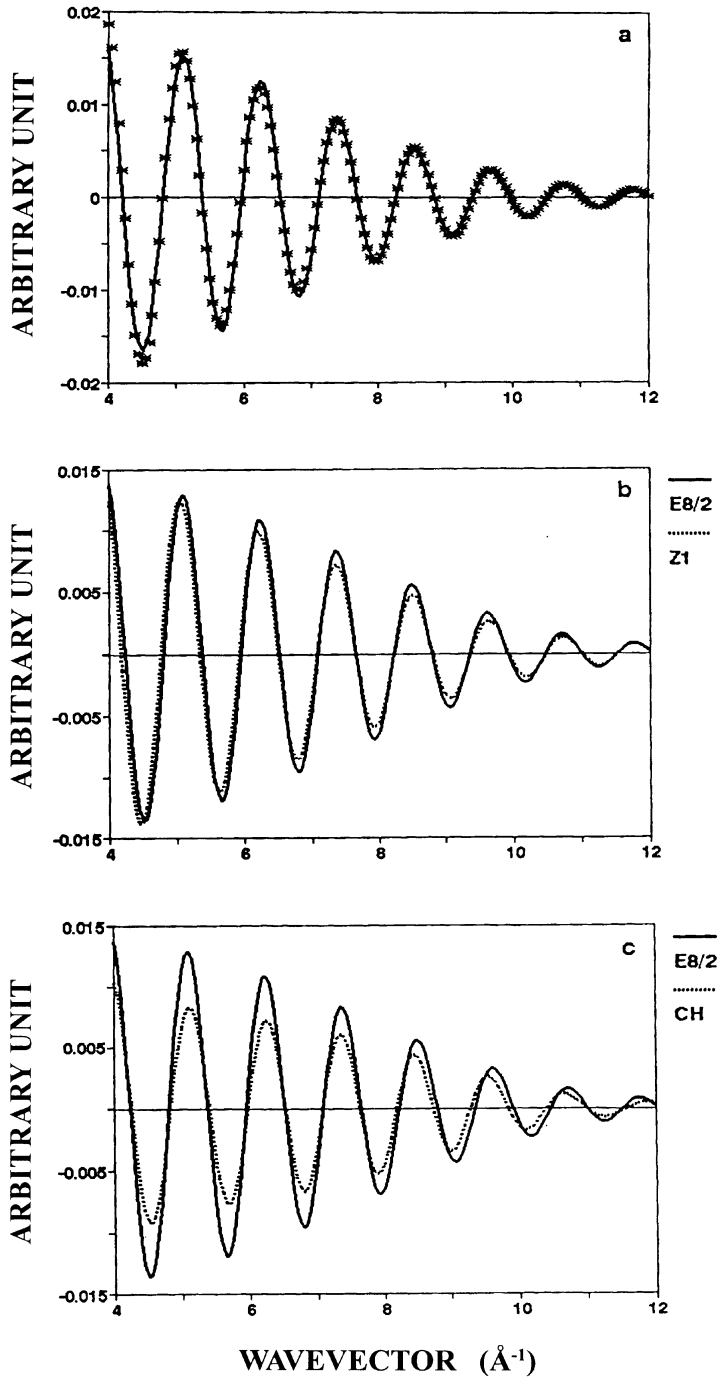

FIG. 2. Fit of the partial EXAFS spectrum corresponding to the second peak of the RDF for reference sample, 69 (a, experimental points are represented by * symbols), and comparison of the partial EXAFS spectra for samples having the same values of N_{Fe} but different N_{Fe}^{r} (b, samples E8/2 and Z1) and for samples having different N_{Fe} values but similar N_{Fe}^{r} (c, samples E8/2 and CH).

Mössbauer spectra were fitted to a series of doublets. Lorentzian line shape was assumed, and all components were assumed to have symmetrical intensities and linewidths.

As can be seen in Table 2, all cation environments around Fe^{3+} may be divided into four groups with the calculated Δ values equal to 0–0.18 mm/s, 0.30–0.45 mm/s, 0.60–0.80 mm/s and above 0.85 mm/s, respectively. In accordance with these values, a number of Fe^{3+} doublets in glauconite Mössbauer spectra may be equal to four. Therefore, each spectrum was first decomposed into two Fe^{3+} doublets and then, if necessary, the number of doublets was increased until an acceptable χ^2 value was obtained (Dainyak & Drits, 1987). Note that the decomposition of the Mössbauer spectrum of sample 68/69 was carried out by Dr Bonnin under conditions when Fe^{3+} isomer shifts have been constrained to be equal.

RESULTS

XRD data

Figure 3 shows XRD patterns typical for the samples studied. The peak positions on these

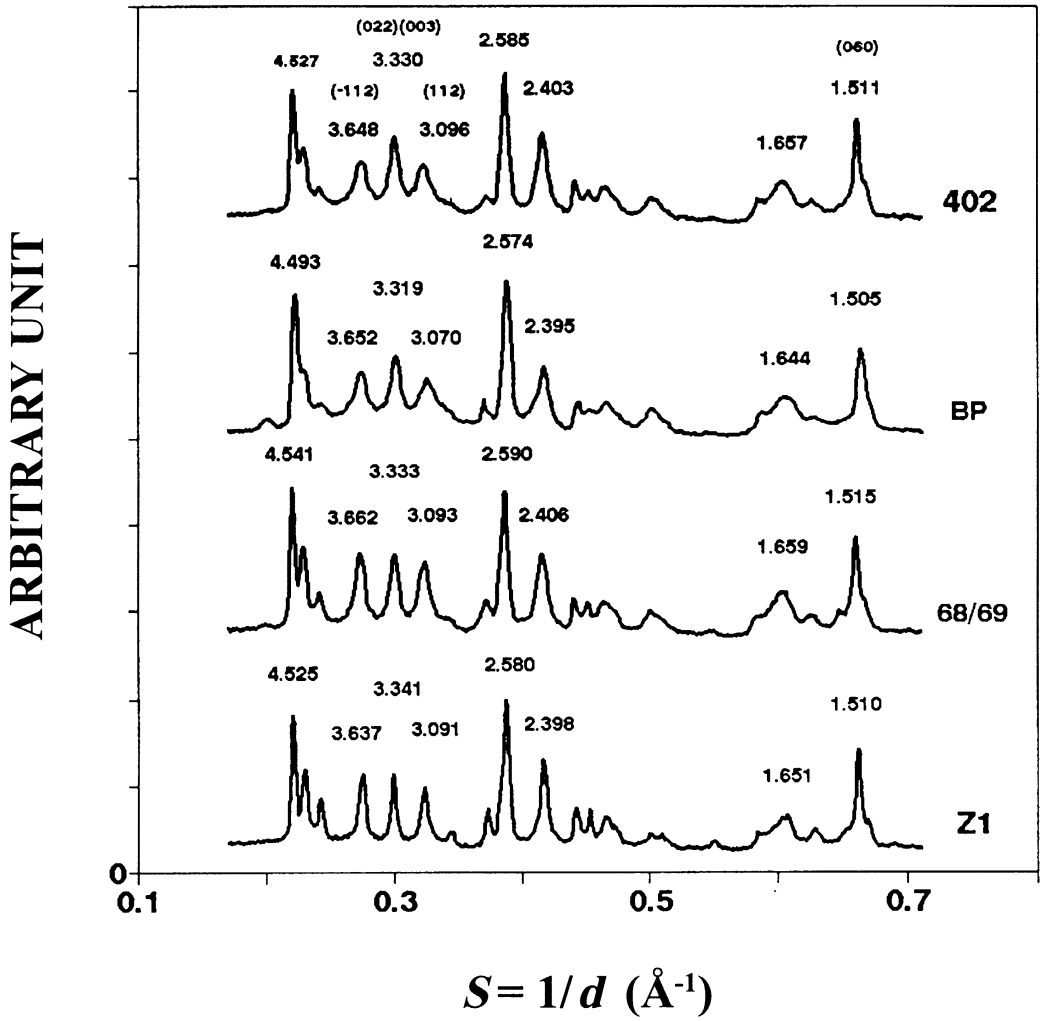

FIG. 3. XRD patterns for samples Z1, 68/69, BP and 402; *hkl* and *d*-values are given above the corresponding peaks.

TABLE 4. Unit-cell parameters b (Å) and $c\cos\beta/a$ calculated from the peak positions of the XRD patterns.

Sample	b (Å)	$c\cos\beta/a$	Sample	b (Å)	$c\cos\beta/a$
Z1	9.06	−0.365	402	9.07	−0.364
69	9.07	−0.359	655	9.09	−0.374
Pil	9.08	−0.373	E8/2	9.07	−0.379
68/69	9.09	−0.374	BP	9.03	−0.385

patterns correspond to those for a monomineral dioctahedral one-layer mica polytype. The observed variations in the reflection intensity and resolution are due to the presence of rotational stacking faults (Sakharov *et al*., 1990). In accordance with the diffraction features for dioctahedral tv 1*M* mica, XRD patterns contain strong $11\bar{1}$, $11\bar{2}$ and 112 reflections, whereas the 111 reflection has zero intensity. Table 4 contains $d(060)$ and $c\cos\beta/a$ values calculated from the peak positions for each sample. For the samples studied the $c\cos\beta/a$ values vary from −0.359 for sample 69 to −0.385 for sample BP. In the case of Fe-free illites, this quantity is equal to −0.40 and −0.3 for tv 1*M* and cv 1*M*, respectively (Drits *et al*., 1993a). Intermediate values correspond to one-layer Fe-free illite structures consisting of interstratified tv- and cv 2:1 layers (Drits & McCarty, 1996). Different values of $c\cos\beta/a$ for the studied samples are determined, however, by specific chemical composition of the samples, containing relatively high contents of Fe^{3+}, Fe^{2+} and Mg. In fact, a peculiar relationship between the unit-cell parameters of tv 1*M* mica, namely, I $c\cos\beta/a$ I >1/3, is determined by a specific distortion of octahedral sheets of 2:1 layers (Bailey, 1984). This distortion is caused by electrostatic interactions between octahedral cations, and depends on octahedral cation composition: the lower charge and the larger size of these cations, the lower electrostatic cation interaction and the smaller distortion of the sheets, i.e. the smaller the deviation of I $c\cos\beta/a$ I from 1/3. The validity of this assumption is illustrated by an almost linear relationship between I $c\cos\beta/a$ I and the total number of divalent octahedral cations as shown in Fig. 4 for the samples studied. The observed intensity distribution implies that all the samples under study have *trans*-vacant octahedra.

IR data

The OH-stretching frequencies and integrated optical densities of individual bands corresponding to definite octahedral cations bonded to OH groups are given in Table 5. Examples of the IR spectra decompositions for several samples are shown in Fig. 5. Table 6 shows the agreement between the octahedral cation contents obtained from the chemical analysis and those calculated from the integrated optical densities.

Table 5 illustrates a wide diversity of values for integrated optical densities reflecting the diversity in the local cation distributions. Even the ratio of $(R^{3+}\text{-}R^{3+})$:$(R^{2+}\text{-}R^{3+})$:$(R^{2+}\text{-}R^{2+})$ cation pairs bonded to OH groups permits us to distinguish at least four groups (Table 5). For these groups, the proportions of these pairs are approximately equal to 1:3:0.5 (samples Z1, 69); 1:1:0.3 (samples E8/2, 655); 1:1:0.125 (samples 68/69, Pil), and 2:1:0.1 (samples CH, BP), respectively. These data show that $R^{3+}\text{-}R^{2+}$ configurations prevail in celadonite

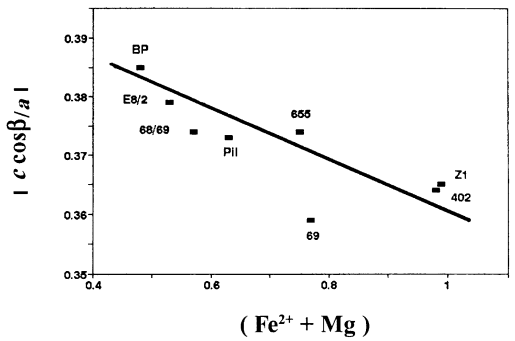

FIG. 4. Relationship between I $c\cos\beta/a$ I and the total amount of divalent octahedral cations for the samples studied.

TABLE 5. OH-stretching frequencies (in cm^{-1}) and optical densities of the bands resulting from the decomposition of the IR spectra studied.

Type of local cation envir.	Pair	Sample Z1	69	Pil	6869	655	E8/2	BP	CH	Freq.
Mica-like	$Fe^{2+}Fe^{2+}$	6.6	5.5	–	–	2.1	–	1.7	–	3505
	$Fe^{2+}Fe^{3+}$	10.4	25.8	19.7	19.0	8.1	5.3	1.1	–	3521
	$Fe^{3+}Fe^{3+}$	13.7	16.0	15.5	18.1	30.4	14.0	12.3	11.6	3535
	$MgFe^{2+}$	3.6	1.6	0.7	–	2.2	4.3	0.3	–	3543
	$AlFe^{2+}$	–	–	–	–	–	–	3.5	7.7	3559
	$MgFe^{3+}$	56.1	32.4	16.2	18.7	27.7	13.3	7.6	–	3559
	$AlFe^{3+}$	2.6	5.6	17.3	17.5	–	10.2	2.6	27.7	3573
	MgMg	3.8	4.4	6.0	4.8	13.4	7.3	2.8	0.8	3583
	AlMg	2.5	2.4	11.5	8.8	6.6	13.1	20.7	25.8	3604
	AlAl	0.7	–	7.6	9.0	6.6	9.5	23.3	4.3	3621
	AlAl	–	–	5.5	4.1	–	–	13.8	17.3	3641
	AlAl	–	–	–	–	–	11.6	–	–	3658
Pyroph.-like	$Fe^{3+}Fe^{3+}$	–	6.3	–	–	2.7	11.3	–	1.0	3631
	$Fe^{3+}Al$	–	–	–	–	–	–	10.3	3.8	3652
	AlAl	–	–	–	–	–	–	–	–	3675
	$R^{3+}R^{3+}$	17	27.9	45.9	48.7	39.7	50.6	62.3	65.4	–
	$R^{3+}R^{2+}$	69	60.6	47.4	46.5	42.4	31.7	32.9	33.8	–
	$R^{2+}R^{2+}$	14	11.5	6.7	4.8	17.9	11.7	4.8	0.8	–

TABLE 6. Octahedral cation contents obtained from the chemical analysis (I) and calculated from the integrated optical densities (II).

Sample		Cation Al	Fe^{3+}	Fe^{2+}	Mg
Z1	I	0.05	0.96	0.26	0.73
	II	0.07	0.96	0.27	0.70
69	I	0.05	1.15	0.36	0.41
	II	0.08	1.08	0.38	0.45
Pil	I	0.44	0.93	0.21	0.42
	II	0.55	0.84	0.20	0.40
68/69	I	0.55	0.89	0.18	0.39
	II	0.52	0.91	0.19	0.37
CH	I	0.92	0.74	0.07	0.27
	II	1.08	0.57	0.08	0.27
655	I	0.16	1.10	0.12	0.63
	II	0.20	1.02	0.15	0.63
E8/2	I	0.68	0.79	0.10	0.43
	II	0.66	0.79	0.10	0.45
BP	I	1.11	0.41	0.13	0.35
	II	1.11	0.46	0.08	0.34

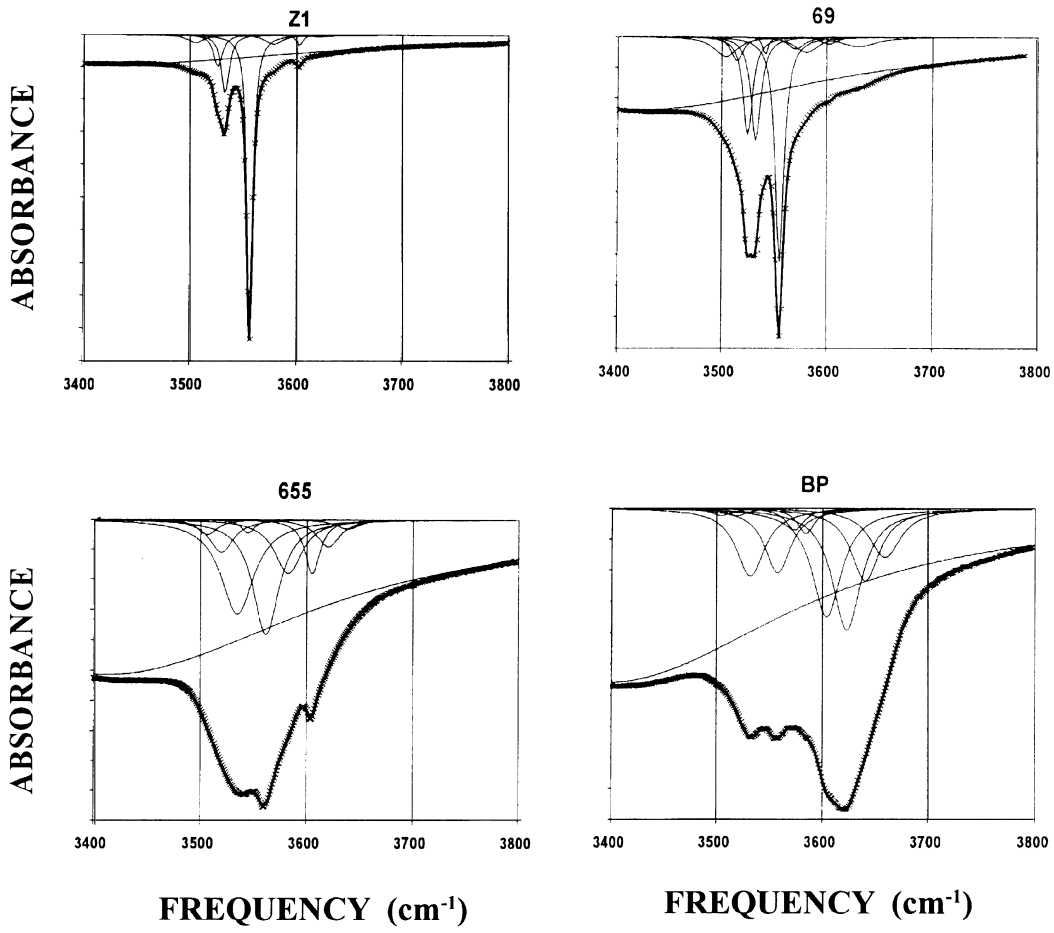

FIG. 5. IR spectra decompositions for samples Z1, 69, 665 and BP.

samples containing approximately equal numbers of R^{3+} and R^{2+} cations. Decrease in the number of divalent cations to 0.7–0.5 atoms per unit-cell equalizes proportions of R^{3+}-R^{3+} and R^{3+}-R^{2+}, but different samples differ in contents of R^{2+}-R^{2+}. Table 5 shows that for most samples, $W_{(Fe2+Fe2+)}$ is zero or very small. On the contrary, the W_{MgMg} values vary within wider intervals, which reflects different degrees of HCD. The fourth group containing the highest amount of octahedral trivalent cations with prevalence of Al, the proportion of R^{2+}-R^{2+} pairs is the lowest. Some samples contain pyrophyllite-like local Fe^{3+}-OH-Fe^{3+} (samples 69, 655, E8/2) and Fe^{3+}-OH-Al (samples CH and BP) fragments.

Some samples have similar chemical compositions but quite different integrated optical densities for the same cation pairs. For example, samples CH and BP have Fe-illite composition, but the first sample is characterized by a high occurrence probability for Al-OH-Fe^{3+} and Al-OH-Mg combinations, whereas in the second one, the Al-OH-Al local environments prevail (Table 5). Samples Z1 and 655 also have similar octahedral cation contents but different values of (W_{ij} + W_{ji}) for the same cation pairs. For example, in sample Z1, the occurrence probability for Mg-Fe^{3+} is >50%, whereas in sample 655, this probability is twice as low because of the distinct increase in the number of Fe^{3+}-Fe^{3+} and Mg-Mg cation pairs (Table 5).

EXAFS data

The RDFs for the series of samples are compared in Fig.6. Emphasis will be placed on the second RDF peaks, which correspond to the contribution of nearest Fe-(Fe,Mg,Al) and Fe-(Si,Al) atomic shells at 3.0–3.3 Å. Since the contribution of the tetrahedral sheets is the same for all compounds, changes in the intensity of these peaks characterize variations in the $N_{Fe\text{-}Fe}$: $N_{Fe\text{-}(Mg,Al)}$ ratio. However, it is impossible to draw definite conclusions merely on the basis of peak intensities, as these RDFs correspond to the modulus of the Fourier transform, the imaginary part not being represented. More detailed information is provided by comparing the contribution to EXAFS of these nearest cationic shells obtained by backtransforming these second RDF peaks to k space. A selection of these contributions is shown in Fig. 2b and 2c. Noteworthy is the spectral similarity for E8/2 and Z1 samples despite a considerable difference in their chemical composition. On the other hand, samples CH and E8/2 have distinct line shapes despite the similarity of their chemical composition. These two examples indicate that N_{Fe} is not always proportional to the Fe content. The structural results are reported in Table 7. The N_{Fe} varies from 0.96 (sample CH) to 2.56 (sample 402). This Table also

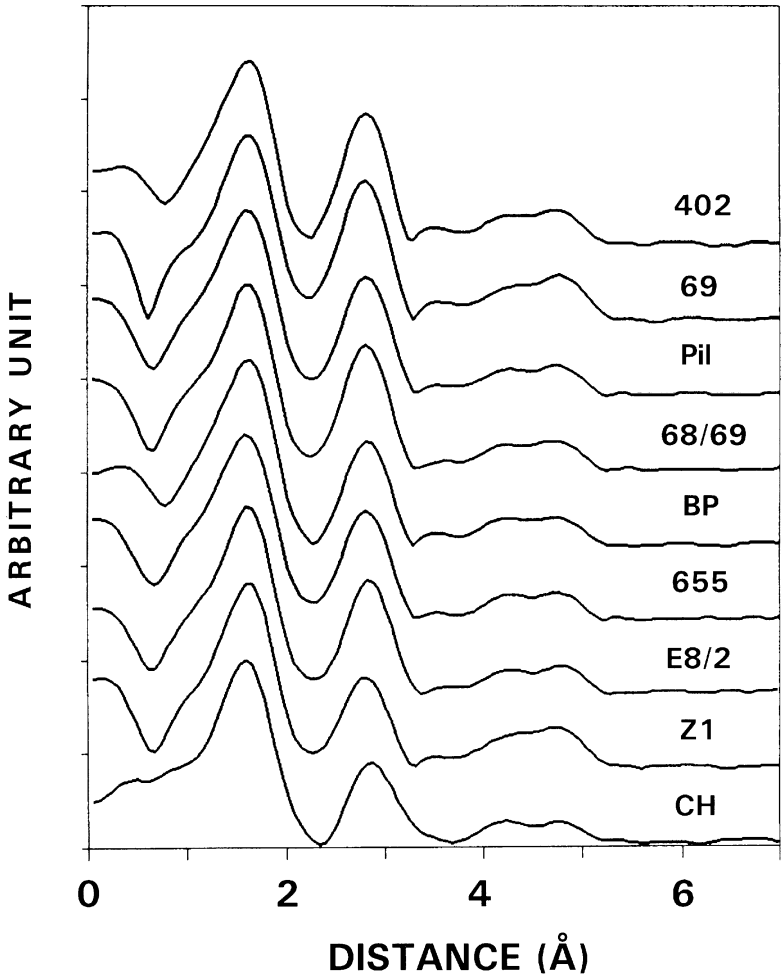

FIG. 6. Radial distribution functions for the samples under study.

TABLE 7. EXAFS parameters resulting from the sample EXAFS spectra analysis.

Sample	Atomic pair	N	R (Å)	σ (Å)	χ^2	N_{Fe}^r
Z1	Fe - Fe	1.5	3.018	0.09		
	Fe - (Mg,Al)	1.47	3.018	0.09	4.10^{-5}	1.83
69	Fe - Fe	2.20	3.022	0.09		
	Fe - (Mg,Al)	0.80	3.022	0.09	1.10^{-5}	2.26
Pil	Fe - Fe	1.97	3.028	0.09		
	Fe - (Mg,Al)	1.00	3.028	0.09	$6.10-5$	1.71
68/69	Fe - Fe	1.90	3.030	0.08		
	Fe - (Mg,Al)	1.10	3.030	0.08	8.10^{-6}	1.60
402	Fe - Fe	2.56	3.022	0.10		
	Fe - (Mg,Al)	0.50	3.022	0.10	5.10^{-6}	1.56
CH	Fe - Fe	0.96	3.022	0.07		
	Fe - (Mg,Al)	2.10	3.022	0.07	5.10^{-5}	1.21
655	Fe - Fe	1.63	3.030	0.08		
	Fe - (Mg,Al)	1.35	3.030	0.08	2.10^{-5}	1.82
E8/2	Fe - Fe	1.51	3.022	0.06		
	Fe - (Mg,Al)	1.50	3.022	0.06	1.10^{-5}	1.33
BP	Fe - Fe	1.77	3.010	0.10		
	Fe - (Mg,Al)	1.25	3.010	0.10	3.10^{-6}	0.81

N: number of cations in the first cationic shell.
R: interatomic distance.
σ: Debye-Waller parameter.
N_{Fe}^r: number of cations corresponding to a random distribution of Fe.
For all spectra ΔE_0 varied from −1.5 eV to 1.5 eV.
The following parameters were fixed during the fitting procedure:
$\Gamma = 1.7$ Å^{-2} (except for sample 69)
$N_{Si} = 4$
$R_{Fe\text{-}Si} = 3.23$ Å

contains the N_{Fe}^r values corresponding to random distribution of Fe^{3+} and Fe^{2+} over the available sites when $N_{Fe}^r = 3W_{Fe}$, and where W_{Fe} is the fractional amount of Fe cations per octahedral site, as determined from the structural formulae (Table 3). A glance at Table 7 shows that in most samples, the difference between N_{Fe} and N_{Fe}^r does not exceed $\pm 10-20\%$. In general, there is a good agreement between the EXAFS and IR results. For example, the N_{Fe} values show that in sample CH (N_{Fe} = 0.96), the distribution of Al and Fe is more uniform than in sample BP (N_{Fe} = 1.77). Samples 655 and BP have quite distinct Fe^{3+}+Fe^{2+} contents but similar N_{Fe} values, 1.63 and 1.77 respectively. Again, in agreement with the IR data, one may conclude that Al and Fe cations are segregated in sample BP.

Mössbauer spectroscopy data

Figure 7 shows Mössbauer spectra for several studied samples (Z1, 655, Pil, 68/69), and Table 8 contains Mössbauer parameters obtained from the spectra decomposition. Figure 7 and Table 8 show that the spectra were fitted with three (655 and Pil samples) and four (Z1, 68/69 and BP samples) quadrupole doublets of Fe^{3+}. Each doublet is characterized by a definite interval of values of the quadrupole splitting, Δ: the interval of minimum Δ values from 0.16 mm/s to 0.18 mm/s is denoted by A, the intervals from 0.33 to 0.45 mm/s and from 0.61 to 0.80 mm/s are denoted by B and C, respectively. The interval of the maximum Δ values from 1.07 to 1.20 mm/s is denoted by D. Table 8 shows that the Fe^{3+} doublets of the Mössbauer

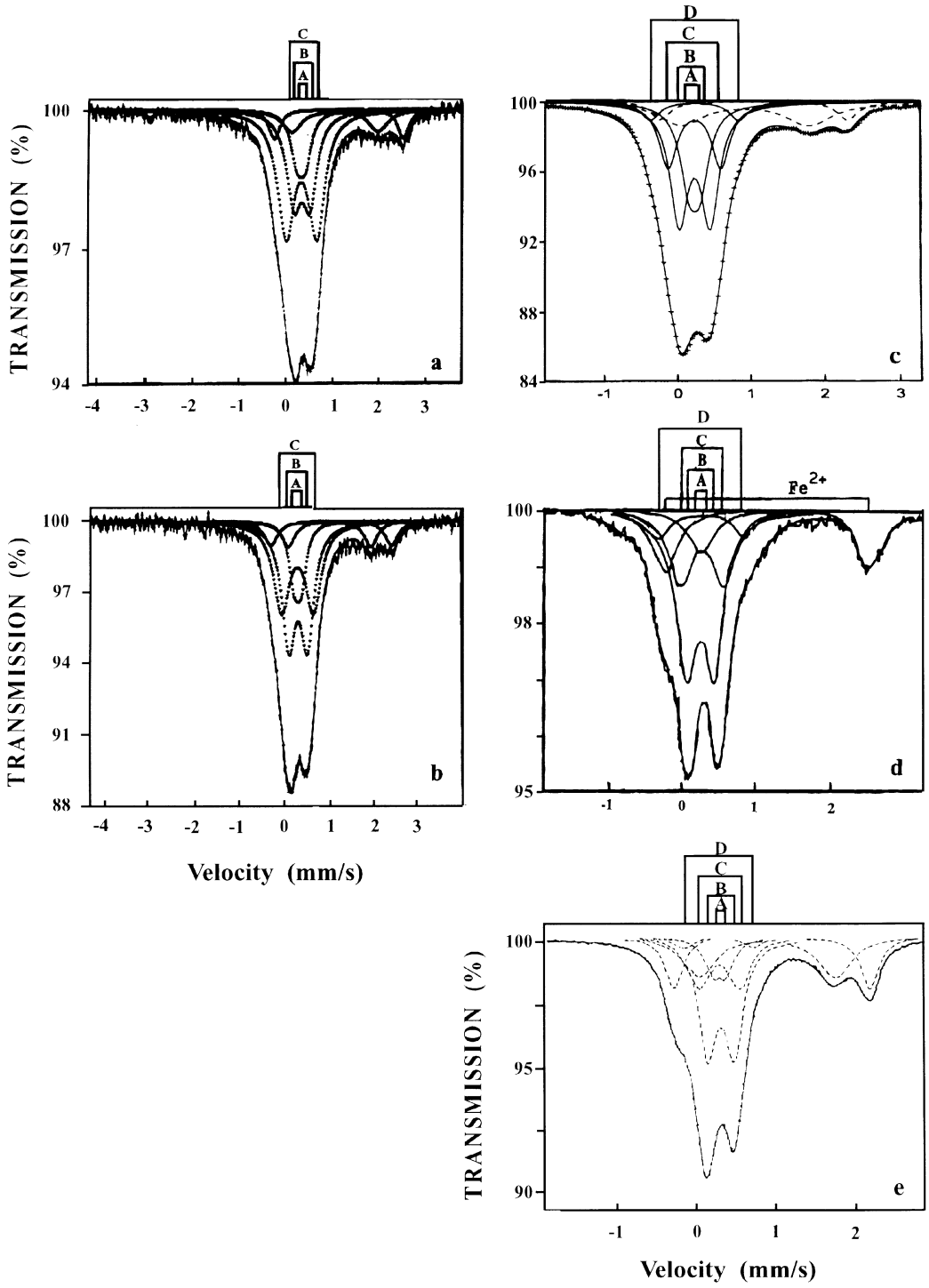

FIG. 7. Mössbauer spectra and their computer fitting for samples 655 (a), Pil (b), 68/69 (c), Z1 (d), and BP (e).

TABLE 8. Mössbauer parameters for the studied samples at 300 K.

Sample	δ(mm/s)	Δ(mm/s)	FW(mm/s)	I(%)	Assignment
	0.35	0.18	0.29	12	Fe^{3+}-A
	0.36	0.33	0.37	27	Fe^{3+}-B
655	0.34	0.64	0.42	44	Fe^{3+}-C
	1.14	2.70	0.29	7	Fe^{2+}-II
	1.06	1.80	0.51	10	Fe^{2+}-I
	0.36	0.16	0.26	13	Fe^{3+}-A
	0.36	0.41	0.36	38	Fe^{3+}-B
Pil	0.35	0.70	0.43	33	Fe^{3+}-C
	1.10	2.66	0.37	8	Fe^{2+}-II
	1.07	1.82	0.36	8	Fe^{2+}-I
	0.30	0.18	0.27	7	Fe^{3+}-A
	0.30	0.37	0.27	44	Fe^{3+}-B
Z1	0.30	0.59	0.27	20	Fe^{3+}-C
	0.31	1.15	0.27	10	Fe^{3+}-D
	1.07	2.25	0.38	19	Fe^{2+}-II
	0.34	0.16	0.29	20	Fe^{3+}-A
	0.34	0.42	0.29	32	Fe^{3+}-B
68/69	0.34	0.72	0.29	19	Fe^{3+}-C
	0.34	1.21	0.29	5	Fe^{3+}-D
	1.05	1.73	0.75	18	Fe^{2+}-I
	1.14	2.54	0.31	6	Fe^{2+}-II
	0.37	0.19	0.28	7	Fe^{3+}-A
	0.37	0.39	0.38	37	Fe^{3+}-B
BP	0.37	0.60	0.38	16	Fe^{3+}-C
	0.40	1.08	0.40	3	Fe^{3+}-D
	1.07	1.92	0.57	22	Fe^{2+}-I
	1.14	2.82	0.30	15	Fe^{2+}-II

δ: isomer shift *vs.* α-Fe.
Δ: quadrupole splitting.
FW: full width at half-maximum.
I: relative peak area.
For all spectra χ^2 values varied within 1.1−1.3.

spectra obtained in the same experimental conditions are characterized by similar values of isomer shift, δ. Each of A, B, C or D doublets corresponding to the Mössbauer spectra of different samples is characterized by similar values of quadrupole splitting, Δ. One or two Fe^{2+} doublets were observed in the Mössbauer spectra and described by one or two sets of parameters (Fig. 7 and Table 8). Structural interpretation of these doublets is unclear.

Octahedral cation distribution models simulated on the basis of the IR data

Analysis of octahedral cation distributions includes the following steps: computer simulation of possible cation distributions using IR data and calculation of the occurrence probabilities for Fe^{3+} having different nearest octahedral cations; choice of the distributions having the values of N_{Fe} that are close to those determined by EXAFS; assignment of each local cation configuration around Fe^{3+} to the predicted Δ values (Table 2); dividing the cation configurations into four groups depending on the Δ values, in accordance with the A, B, C, and D doublets in the analysed Mössbauer spectrum; calculation of the occurrence probabilities W_A, W_B, W_C and W_D for each group of cation arrangements; within each group, calculation of the statistically weighted quadrupole splitting as a sum of products of the

TABLE 9. The N_{Fe} values for the different models of cation distribution on the basis of IR data.

Model		Sample Z1	69	Pil	6869	CH	655	E8/2	BP
Random		1.86	2.28	1.57	1.65	0.97	1.83	1.33	0.83
'equiv'	'cons'	1.73	2.19	1.71	1.77	1.03	1.94	1.57	1.09
	$\alpha = 0$	1.76	2.24	2.05	2.10	1.62	–	1.99	1.67
	$\alpha = 0.5$	1.56	2.16	1.99	2.05	1.60	1.87	1.93	1.65
	$\alpha = 0.5$ S = 30,000	1.51	2.14	2.02	2.17	1.80	1.78	1.99	1.87
	$\alpha = 1$	1.55	2.13	1.68	1.76	1.03	–	1.53	1.09
	$\alpha = 1$ S = 30,000	1.48	2.08	1.67	1.79	1.08	–	1.57	1.06
'pref'	'cons'	1.47	2.12	1.64	1.74	1.02	1.91	1.56	1.11
	$\alpha = 0$	1.49	2.16	1.99	2.04	1.59	–	1.98	1.63
	$\alpha = 0.5$	1.43	2.12	1.94	2.03	1.60	1.84	1.93	1.69
	$\alpha = 0.5$ S = 30,000	1.42	2.10	2.05	2.04	1.83	1.77	2.03	1.93
	$\alpha = 1$	1.42	2.10	1.68	1.73	1.02	–	1.52	1.07
	$\alpha = 1$ S = 30,000	1.39	2.07	1.68	1.72	1.04	–	1.51	1.14

occurrence probability and the individual quadrupole splitting; comparison of the weighted quadrupole splittings with the corresponding Δ values determined from the Mössbauer spectrum decomposition for the sample under study; and comparison of areas of the A, B, C, and D doublets determined from Mössbauer spectrum decomposition with the occurrence probabilities W_A, W_B, W_C and W_D calculated from the cation distribution model under consideration.

To make it clear, let us consider as an example the application of this procedure to the determination of a cation distribution for sample Z1. Table 9 contains N_{Fe} values calculated for the cation distributions simulated on the basis of the IR data. The value for N_{Fe} determined for sample Z1 from EXAFS is 1.52 (Table 7). Table 9 shows that several quite different cation distributions are characterized by similar N_{Fe} values. Analysis of these distributions has shown that the one shown in Fig. 8a with $N_{Fe} = 1.47$ is closely correlated with the Mössbauer data of the sample. In this distribution, R^{2+} cations occupy only one of the two symmetrically independent *cis*-sites (the condition: 'pref'), and there are no other limitations for the nearest neighbourhood of different cation types.

Table 10 contains all local arrangements around Fe^{3+} which occur in this distribution. They are grouped into four groups in accordance with the predicted quadrupole splittings, Δ^{cal}, as well as with the Δ^{exp} values determined for the A, B, C and D doublets of Fe^{3+} revealed in the Mössbauer spectrum. The third and the fourth columns of Table 10 contain the occurrence probabilities or 'weights' for each individual cation environment within each group and within the whole distribution, respectively. It is easy to calculate the sum of the products of Δ^{cal} and the corresponding 'weights' within each group. These values are 0.15 mm/s, 0.35 mm/s, 0.63 mm/s and 0.91 mm/s, and correlate quite well with experimental ones, namely 0.18 mm/s, 0.37 mm/s, 0.59 mm/s and 1.15 mm/s. The total 'weight' of each group is equal to the sum of 'weights' of individual cation arrangements around Fe^{3+} determined for the whole distribution. These model values are equal to 14.2%, 55.4%, 25.9% and 4.5% whereas the areas under the corresponding A, B, C and D doublets in the Mössbauer spectrum are 8.4%, 54.4%, 25.3% and 11.9%, respectively.

Taking into account that in sample Z1 the ratio of $R^{3+}/R^{2+} \approx 1$, it was natural to expect that octahedral cations should be distributed with a high degree of HCD, when each R^{2+} has three nearest R^{3+} cations and vice versa. In fact, the cation distribution is characterized by the presence of a considerable number of 'faults' violating the expected distribution. Table 10 shows that only

TABLE 10. Contents of cation arrangements around Fe^{3+} within the A, B, C and D groups (the fourth column) and within the whole cation distribution for Z1 sample (the fifth column). The third column contains values of quadrupole splitting calculated for each arrangement.

Group	Arrangements	Δ^{cal} (mm/s)	Contents within the group	Contents within the whole distribution
A	$3Fe^{3+}$	0.17	0.59	0.080
	$2Fe^{2+}Mg$	0.13	0.41	0.055
B	$2MgFe^{2+}$	0.26	0.33	0.182
	$2Fe^{2+}Fe^{3+}$	0.31	0.01	0.007
	$Al2Fe^{3+}$	0.33	0.02	0.011
	3Mg	0.39	0.47	0.259
	$Al2Fe^{2+}$	0.44	0.01	0.004
	$MgFe^{2+}Fe^{3+}$	0.44	0.16	0.091
C	$2Fe^{3+}Fe^{2+}$	0.59	0.10	0.027
	$AlFe^{2+}Mg$	0.58	0.05	0.013
	$2MgFe^{3+}$	0.58	0.53	0.137
	2MgAl	0.72	0.10	0.027
	$AlFe^{3+}Fe^{2+}$	0.74	0.04	0.011
	$2Fe^{3+}Mg$	0.74	0.18	0.044
D	$AlMgFe^{3+}$	0.89	0.85	0.045
	2AlMg	1.05	0.15	0.008

50% of the local arrangements around Fe^{3+} correspond to $3R^{2+}$. The main reason for this is that the 2:1 layers contain $\sim$17% of R^{3+}-OH-R^{3+} pairs (Table 5), that is, under this restriction, it is impossible to provide occupancy of the symmetrically independent *cis*-sites by only R^{2+} and to avoid violation of the HCD. Nevertheless, as seen in Fig. 8a, within the whole cation distribution, there are large domains in which strict HCD is fulfilled. These domains are separated by small regions in which either R^{3+} or R^{2+} prevails.

The same approach was applied to samples 655, Pil, 68/69 and BP. Table 11 compares the Δ values and 'weights' for the A, B, C and D doublets determined by the decomposition of the Mössbauer spectra and by the simulated cation distribution satisfying this decomposition. Table 11 shows that, in general, the agreement between the experimental parameters and those calculated for the chosen simulated models is quite acceptable. Note the main features in the final cation distributions for the other samples.

Sample Pil. According to the chemical composition, the number of R^{3+} cations is twice as high as that of R^{2+}, and ratios of Fe^{3+} to Al and Mg to Fe^{2+} (Table 1) are also equal to two. The IR spectrum decomposition has shown that Fe^{3+}-Fe^{3+}, Al-Fe^{3+}, Fe^{3+}-Mg, Fe^{3+}-Fe^{2+}, Al-Mg cation pairs occur with similar probabilities (Table 5). The value of N_{Fe} determined from the EXAFS spectrum is equal to 1.97. Table 9 shows that this value corresponds to several different cation distributions. The cation distribution that satisfies the Mössbauer spectrum decomposition is characterized by the following restriction conditions: 'pref', α = 0.5, S = 30,000, N_{Fe}^{cal} = 2.05 (Table 11). It means that in this model, the R^{2+} cations occupy only one of the two symmetrically independent *cis*-sites and R^{2+}-R^{2+} and Al-Fe^{3+} pairs in the b_1 and b_2 directions are forbidden (α = 0.5). In addition, 30,000 attempts were made to minimize the penalty function f(α). As seen in Fig. 8b, the cation distribution is represented by three types of domains differing in cation composition. One of the domain types consists almost completely of Al, the second one is represented by Fe only, and the third contains a mixture of Fe and Al.

Sample 68/69. The chemical compositions and the results of the IR spectrum decompositions are quite similar to those for sample Pil (Tables 3 and 5). The N_{Fe} values are also very close; 1.90 and 1.97 for samples 68/69 and Pil, respectively. It is

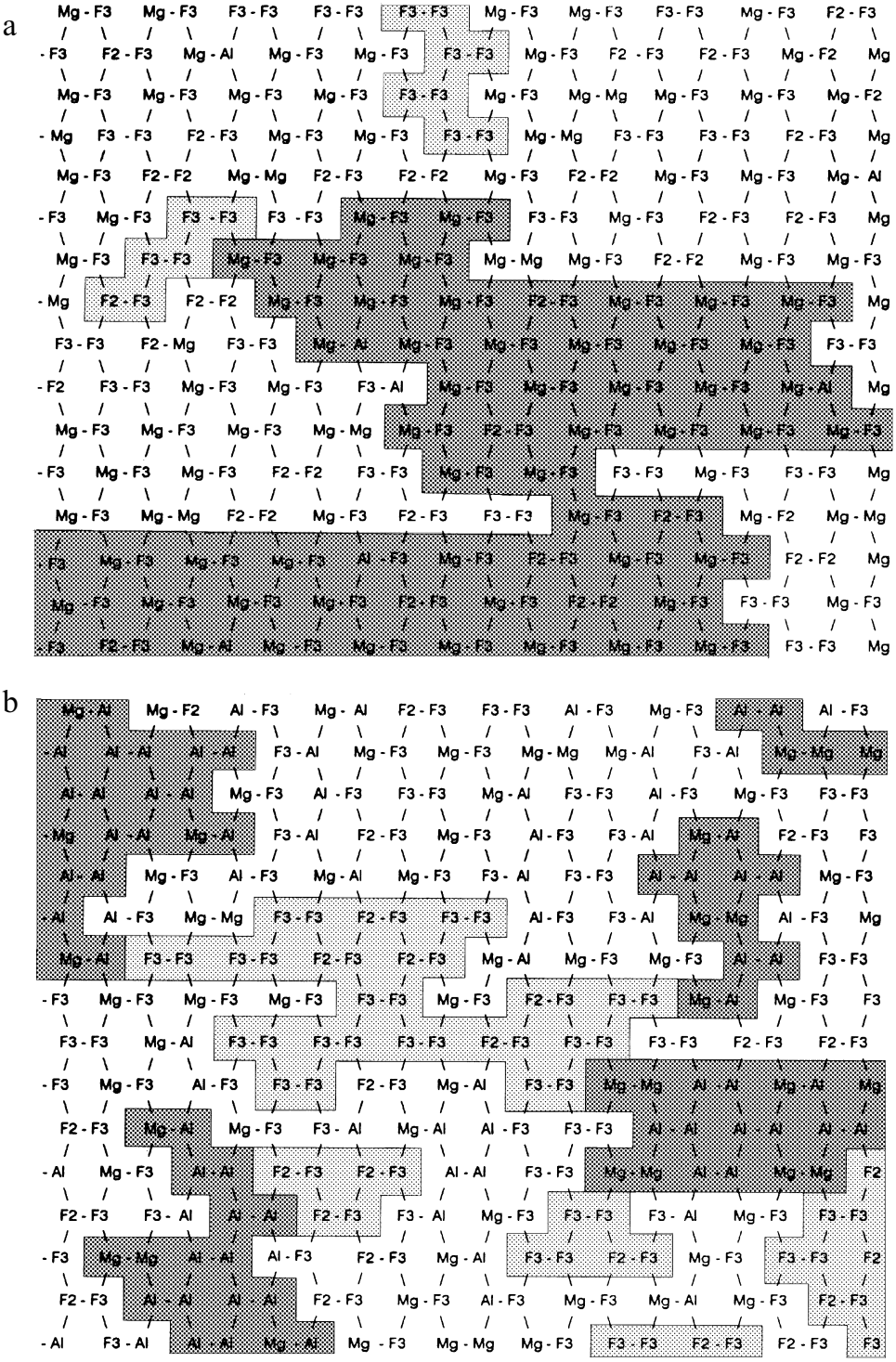

FIG. 8. Two-dimensional cation distributions determined for samples Z1 (a), Pil (b), 68/69 (c), 655 (d) and BP (e).

c

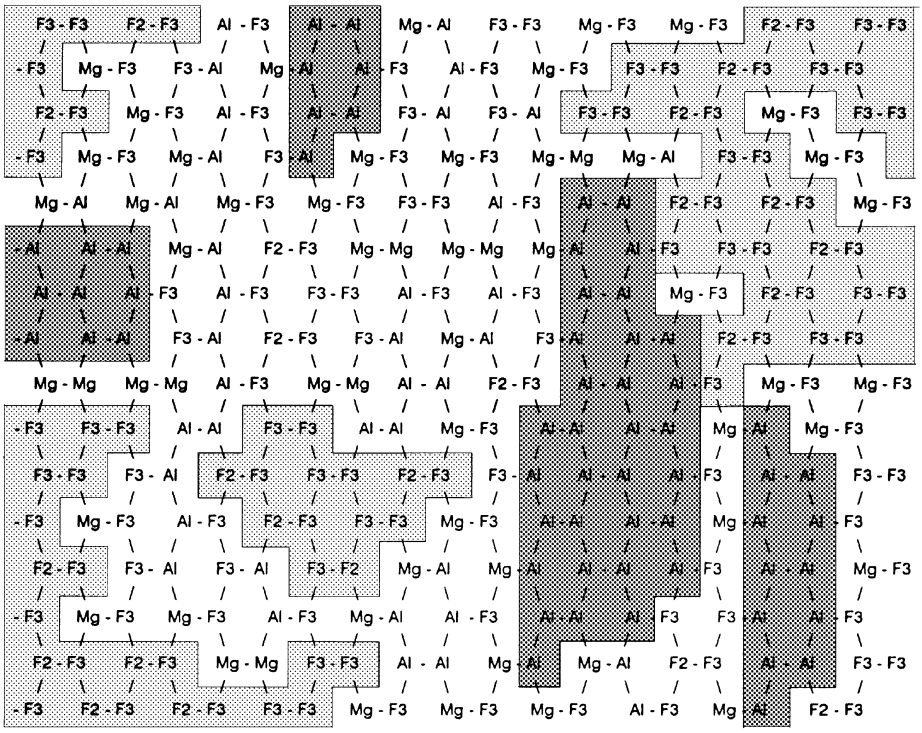

d

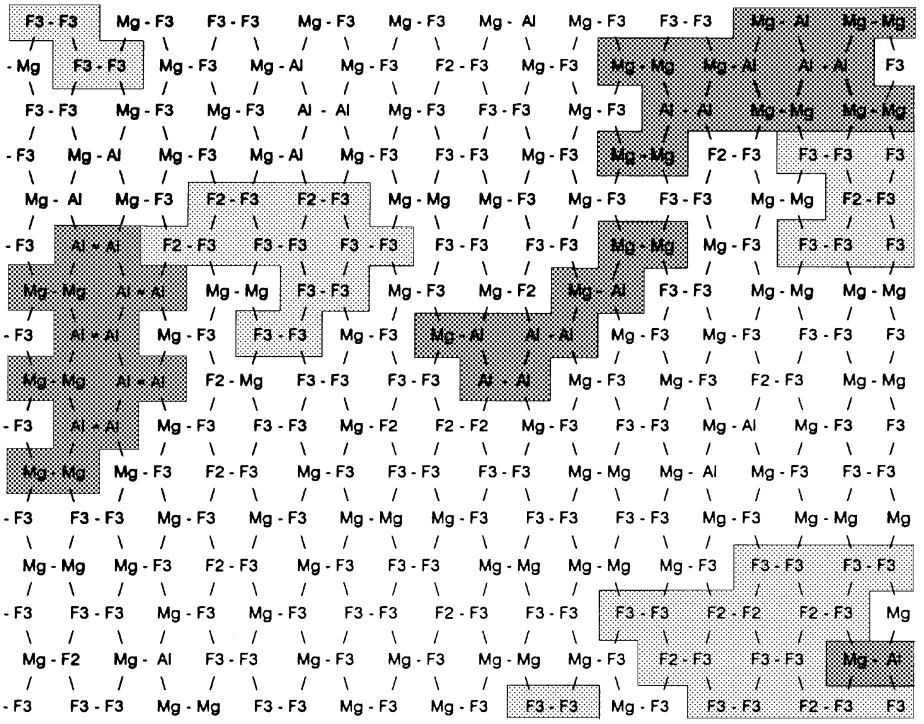

FIG. 8 (contd).

e

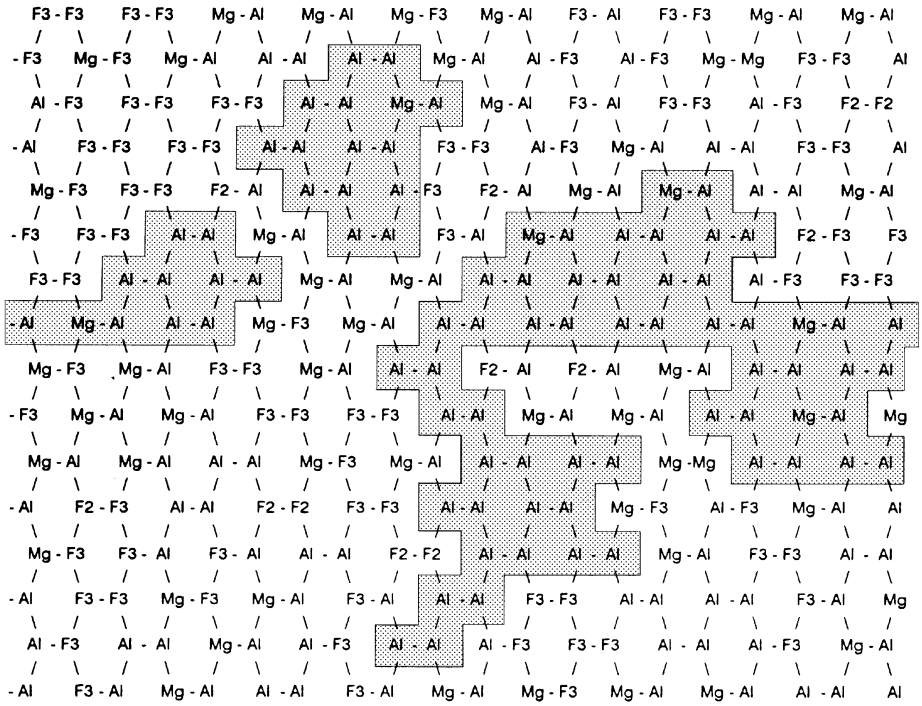

FIG. 8 (contd).

natural that the cation distribution for this sample is characterized by similar restriction conditions ('pref', α = 0.5), as well as by domain structure (Fig. 8c).

Sample 655. The number of octahedral R^{3+} cations is 1.5 times greater than that of R^{2+}, and among them, Fe^{3+} prevails (Table 3). The main OH bands in the IR spectrum correspond to Fe^{3+}-Fe^{3+} (30.4%), Mg-Fe^{3+} (27.7%) and Mg-Mg (13.4%) cation pairs (Table 5). Computer simulation has shown that for these initial data, N_{Fe} remains pratically the same for quite distinct cation distributions (Table 9). For example, N_{Fe} = 1.83 was obtained for random cation distribution; this parameter had its maximum value (1.94) for the restriction conditions: 'equiv', 'cons', and the minimum one (1.77) for the conditions: 'pref', α = 0.5, S = 30,000. The N_{Fe} value determined from EXAFS is 1.63. All attempts to obtain cation distribution with this N_{Fe} value failed. The cation distribution that satisfies the decomposition of the Mössbauer spectrum is characterized by the restriction conditions: 'pref', α = 0.5, and N_{Fe} = 1.85 (Table 11). One of the characteristic features of this cation distribution is a considerable violation of the HCD principle. The main reason for this is the presence of a high content of Mg-OH-Mg cation pairs (13.4%). Minimum deviation from the Pauling rule is achieved by cation arrangements, in which R^{2+}-OH-R^{2+} cation pairs are surrounded by R^{3+}-OH-R^{3+} pairs having the same orientation. Such arrangements appear to be due to the prohibition of R^{2+}-R^{2+} cation pairs along the b_1 and b_2 directions. It should be noted that domains of different cation compositions (if they exist) have very small sizes.

Sample BP. This sample differs from the others in the amount of octahedral Al. The IR data have shown that, along the *b* axis, the cation distribution is characterized by high proportions of trivalent cation pairs: 37.1%, 12.3% and 12.9% for Al-Al, Fe^{3+}-Fe^{3+} and Al-Fe^{3+}, respectively. Note the dramatic difference between N_{Fe} determined from the EXAFS spectrum (N_{Fe} = 1.77) and that calculated from the chemical composition for the random Fe distribution. Table 9 shows that the cation distribution with the highest N_{Fe}^{cal} = 1.63 has been achieved for the restriction conditions: 'pref' and α = 0; that

is, R^{2+}-R^{2+} pairs are prohibited in the b_1 and b_2 directions. The characteristic feature of this distribution is its domain structure. One of the domains consists almost completely of Al while the other contains a mixed cation composition (Fig. 8e).

DISCUSSION

Table 11 shows that the models for cation distribution established in the samples under study were simulated under similar conditions: R^{2+} cations prefer to occupy one of two symmetrically independent *cis*-sites in order to maximize the local compensation of anion charges. In addition, R^{2+}-R^{2+} and/or Al-Fe^{3+} are prohibited in the b_1 and b_2 directions. Under these conditions, the octahedral sheets of Pil, BP and 68/69 samples show domain structure, i.e. they are represented by domains of almost pure Al or Fe^{3+} compositions and by domains of mixed cation composition. The domains differ in size and may contain either a few cations or a few unit-cells (Figs. 8a–e). In domains of mixed cation composition, non-equivalence of 'I' and 'II' *cis*-sites with respect to R^{2+} and R^{3+} occupancy takes place in celadonite-like domains with a high tendency to HCD. Note that in celadonite-like domains, local charge compensation is achieved either conventionally when each R^{3+} is surrounded by three nearest R^{2+}, or by formation of local cation arrangements in which an R^{2+}-OH-R^{2+} pair has R^{3+}-OH-R^{3+} pairs in its nearest environments. In the latter case, each R^{2+} cation is surrounded by two R^{3+} and one R^{2+} nearest cations. Fragments of both types of local cation distribution are shown in Figs. 8a–c. However, the actual cation distribution of sample Z1 (Fig. 8a) is characterized by large domains having the maximum possible homogeneous charge distribution. This result is in agreement with the crystal structure refinement of the sample obtained by oblique texture electron diffraction (Drits *et al*., 1984b). It was shown that the mean cation composition of *cis* I- and *cis* II-sites were non-equivalent with respect to the R^{2+} and R^{3+} content.

The concept of the domain glauconite structure agrees with the model of Townsend *et al*. (1987) for

TABLE 11. Experimental and calculated values of quadrupole splitting, Δ, and intensities, W_i, of the A, B, C and D doublets of Fe^{3+} determined from the Mössbauer spectra decomposition and computer simulation.

Sample			Doublet A	B	C	D
655	Δ (mm/s)	exp	0.18	0.33	0.64	–
		cal	0.16	0.38	0.67	–
	W_i(%)	exp	14.4	32.7	52.9	–
		cal	15	32	53	–
Pil	Δ (mm/s)	exp	0.16	0.41	0.70	–
		cal	0.16	0.43	0.68	–
	W_i(%)	exp	15.6	44.7	39.7	–
		cal	22	43	29	6
Z1	Δ (mm/s)	exp	0.18	0.37	0.59	1.15
		cal	0.15	0.35	0.63	0.92
	W_i(%)	exp	8.4	54.4	25.3	11.9
		cal	14	55	26	5
68/69	Δ (mm/s)	exp	0.16	0.42	0.72	1.20
		cal	0.15	0.38	0.69	0.98
	W_i(%)	exp	26.0	43.0	24.0	7.0
		cal	23	38	33	6
BP	Δ (mm/s)	exp	0.19	0.39	0.60	1.08
		cal	0.17	0.38	0.67	0.92
	W_i(%)	exp	11.1	58.4	25.4	5.0
		cal	12	58	20	10

the interpretation of ferromagnetic ordering at 1.3 K in glauconite. In their model, Fe^{3+} cations are distributed over *cis*-positions so as to maximize their mutual separation implying the ordered alternation of Fe^{3+} in *cis*-positions, i.e. preference of Fe^{3+} to one of the positions. In addition, the transition to ferromagnetic ordering occurs within a certain temperature interval indicating a non-homogeneous structure. It is the domain structure of glauconite that causes this non-homogeneity.

It is noteworthy that the concept of the domain structure of celadonite-glauconite samples satisfies simultaneously the data for three spectroscopic methods sensitive to different local structural environments: IR data characterize one-dimensional cation distribution along the *b* axis, and Mössbauer and EXAFS spectroscopy results are sensitive to different local Fe arrangements at the three-dimensional level.

It should be noted, however, that the contributions of different methods to the solution of the cation distribution problem are not equivalent. For example, Table 9 shows that the N_{Fe} parameter has a very low sensitivity to quite distinct cation distributions. For example, N_{Fe} values are almost the same for the models differing in the degree of octahedral cation preference to one of the *cis*-sites, I and II. Nevertheless, our experience has shown that the application of the EXAFS technique is useful when it is used in combination with other spectroscopic methods. On the one hand, it is important that the data obtained from the EXAFS spectra do not contradict the results of the others techniques applied to the same sample. In fact, the differences between N_{Fe} values determined from the experimental EXAFS spectra and those calculated from the cation distribution described do not exceed 10%, whereas errors in the determination of these parameters by EXAFS may achieve 20−30%. On the other hand, the data obtained from the EXAFS spectra may help to reveal mica structures having a strong tendency to segregation of Fe. For example, sample 402 was not studied by IR and Mössbauer spectroscopy. However, a distinct difference between $N_{Fe}^{EXAFS} = 2.56$ and $N_{Fe}^{random} = 1.47$ (Table 7) shows that the octahedral sheets of the 2:1 layers of this sample should consist of domains, and one of the domain types is enriched by Fe cations.

The effectiveness of the EXAFS technique for the determination of domain structure in trioctahedral layer silicates has been demonstrated by Manceau & Calas (1986) and by Manceau *et al*. (1990). In Ni-Mg serpentines and kerolites, the distribution of Ni atoms was found to strongly deviate from random distribution, with a size of Ni-rich domains exceeding 20 Å in most of the samples. A departure from random cation distribution was also recognized in trioctahedral micas, but the magnitude of this deviation from the statistical distribution was low. This study represents the first attempt to apply EXAFS spectroscopy to the determination of the distribution of octahedral cations in dioctahedral micas. It shows that the efficiency of the method will be increased substantially if mica references of different chemical compositions and polarized EXAFS technique are applied. Application of mica references with well-known structures and chemical characteristics will refine the values of the absorption parameters. Use of the polarized technique permits us to exclude the contribution to the first cation shell of tetrahedral cations (Manceau *et al*., 1990).

The IR spectroscopy in the region of OH-stretching vibration plays a key role in the determination of the nature of short-range cation order/disorder. Unfortunately, the IR spectra of most glauconite samples are characterized by poor resolution of individual OH bands. At present, the OH frequencies corresponding to different cation pairs are determined unambiguously (Besson & Drits, 1996a). However, the problem of IR spectra decomposition remains rather complicated because of a large number of individual OH bands forming mica IR spectra and of the diversity of band widths. For these reasons, IR data must be always correlated with tetrahedral and octahedral cation compositions determined by chemical analysis. One of the best criteria for the IR result validity is the coincidence of octahedral cation compositions determined by both techniques.

Determination of two-dimensional cation distribution becomes possible with the application of Mössbauer spectroscopy. In this particular case, the interpretation of the Mössbauer spectra was based, on the one hand, on the combination of the IR and EXAFS results with computer simulation of cation distribution, and, on the other hand, on comparison between calculated and experimental values for the quadrupole splittings and weights of the A, B, C and/or D doublets of Fe^{3+}. Table 11 demonstrates the efficiency of eqn. (1) for prediction of quadrupole splittings for the A, B and C doublets corresponding to the analysed cation distributions. The difference between the compared values does not exceed 0.06 mm/s. This is a very good result, if

we take into account the high sensitivity of eqn. (1) to the bond length values, d_i, and a huge number of local cation arrangements around Fe^{3+}, which exist in different proportions in the analysed cation distribution. Of course, the correlation between the calculated and experimental values of Δ for the Fe^{3+} doublets became possible because of the correct determination of the content of each definite cation configuration around Fe^{3+} within each of the A, B and C groups (see Table 10).

Table 11 shows that the experimental values of the quadrupole splittings for the D doublet of Fe^{3+} systematically exceed the corresponding calculated values, on average, by 0.20 mm/s. This means that eqn. (1) does not predict the Δ_{ind}^{cal} values correctly for the cation arrangements around Fe^{3+} that are combined into the D group (Table 2). Therefore, in practice, before a fitting, one has to add 0.20 mm/s to the Δ value of the D doublet calculated from the cation distribution analysed.

The difference between the calculated and experimental values of the A, B, C and D doublet weights depends on the weight of the corresponding doublet. Table 11 shows that for the most intense doublets of Fe^{3+}, the relative difference between the compared values seldom exceeds 10%. For low intensity doublets, the relative difference may achieve 100%. This result is not unexpected. Decomposition of poorly resolved glauconite Mössbauer spectra is also a very complicated problem, basically because of the uncertainties in the number and positions of doublets of Fe^{3+} forming the glauconite Mössbauer spectra. Under these conditions, low precision in the determination of weights of weak doublets of Fe^{3+} is expected.

In the light of the results obtained, one can simulate Mössbauer spectra for different cation distributions and compare them with experimental ones. As a matter of fact, for each given cation distribution, we can calculate quadrupole splittings

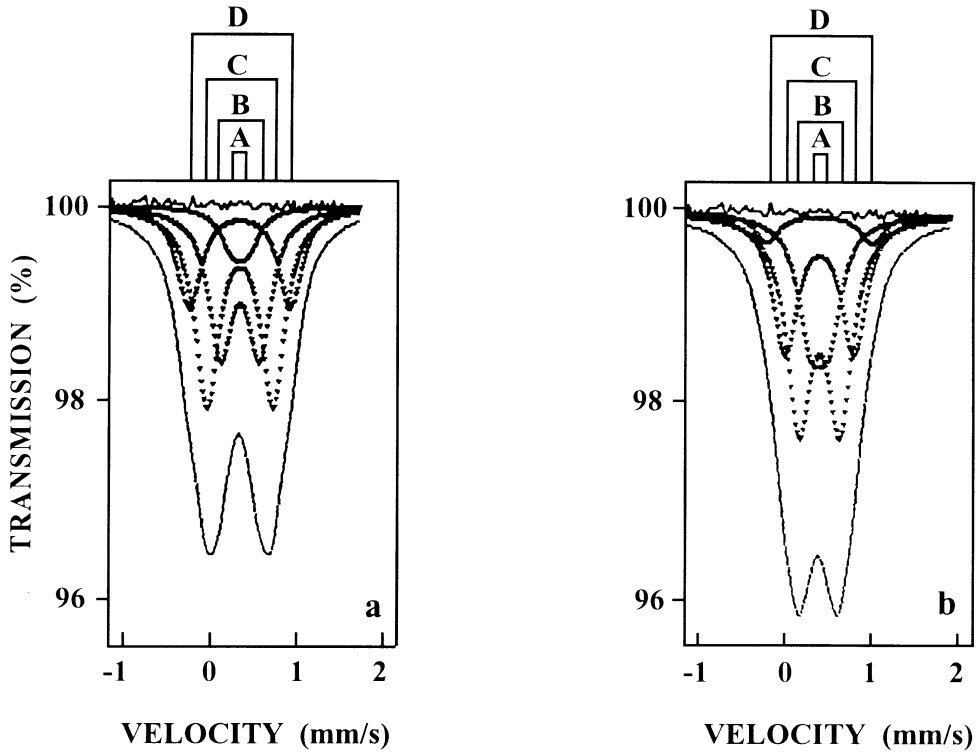

FIG. 9. Simulation of Mössbauer spectra using IR data and different restriction conditions for the cation distributions for sample Pil : (a)'equiv', 'cons'; (b) 'pref', α = 0.5, S = 30,000.

and weights for the A, B, C and D doublets of Fe^{3+}. The main problem still unsolved is the widths of individual doublets. As a first approximation, one may use the value for Γ, similar to those determined experimentally (Table 8), e.g. equal to 0.30 mm/s, 0.35 mm/s and 0.40 mm/s for the A, B and C doublets of Fe^{3+}. Figure 9 shows Mössbauer spectra simulated for sample Pil, whose cation distributions differ in restriction conditions. For each sample, Mössbauer spectra were simulated for two cation distributions first with 'equiv', 'cons', and then with 'pref', $\alpha = 0.5$. In the latter case, the simulated Mössbauer spectrum is similar to the experimental one (Figs. 7b, 9b). Thus, in spite of the poor resolution, glauconite Mössbauer spectra profiles are rather sensitive to considerably different cation distributions.

To conclude, note that the domain structure of glauconites may imply specific formation conditions which may interest geologists and mineralogists. The examples considered, however, do not cover all the diversity of natural glauconites. In order to elucidate whether domain structure is a characteristic feature of glauconites, additional investigations are required. First of all, future development of methodological aspects in the interpretation of experimental spectroscopic data should increase the effectiveness and efficiency of the application of spectroscopic methods to the study of actual cation distribution in mica structures. Improvement of the computer simulation program including additional restrictions on the occurrence probability of various cation types should also promote the successful solution of this problem. Simultaneously, the study of glauconites differing in chemical composition, age and type of source rocks may help to refine a mechanism of glauconite formation.

ACKNOWLEDGMENTS

We thank all the colleagues who supplied us with the samples and Dr D. Bonnin for recording the Mössbauer spectrum. G. Dainyak is grateful to the International and Russian Science Foundations (grant 95-05-14509) for financial support. We are grateful to Drs E. Murad, J.-L. Robert and E. De Grave for their valuable comments on the manuscript.

REFERENCES

Bailey S.W. (1984) Crystal chemistry of the true mica. Pp. 13–60 in: *Micas.* (S.W. Bailey, editor). Reviews in Mineralogy, Mineralogical Society of America, Washington.

Besson G. & Drits V.A. (1997a) Refined relationships between chemical composition of dioctahedral fine-dispersed mica minerals and their infrared spectra in the OH stretching region. Part I: Identification of the stretching bands. *Clays Clay Miner.* **45**, 158–169.

Besson G. & Drits V.A. (1997b) Refined relationships between chemical composition of dioctahedral fine-dispersed mica minerals and their infrared spectra in the OH stretching region. Part II: The main factors affecting OH vibration and quantitative analysis. *Clays Clay Miner.* **45**, 170–183..

Besson G., Drits V.A., Dainyak L.G. & Smoliar B.B. (1987) Analysis of cation distribution in dioctahedral micaceous minerals on the basis of IR-spectroscopy data. *Clay Miner*. **22**, 465–478.

Besson G., Bookin A.S., Dainyak L.G., Rautureau M., Tsipursky S.I., Tchoubar C. & Drits V.A. (1983) Use of diffraction and Mössbauer methods for the structural and crystallochemical characterization of nontronite. *J. Appl. Cryst.* **16**, 374–383.

Bookin A.S., Dainyak L.G. & Drits V.A. (1978) Interpretation of the Mössbauer spectra of layer silicates on the basis of structural modelling. *Phys. Chem. Min.* **3**, 58–59.

Cardile C.M. & Brown I.W.M. (1988) An ^{57}Fe Mössbauer and X-ray diffraction study of New Zealand glauconites. *Clay Miner.* **23**, 13–25.

Dainyak L.G. & Drits V.A. (1987) Interpretation of the Mössbauer spectra of nontronite, celadonite, and glauconite. *Clays Clay Miner.* **35**, 363–372.

Dainyak L.G., Bookin A.S. & Drits V.A. (1984a) Interpretation of Mössbauer spectra of dioctahedral Fe^{3+}-containing 2:1 layer silicates. II. Nontronite. *Kristallografiya*, **29**, 304–311 (in Russian).

Dainyak L.G., Bookin A.S. & Drits V.A. (1984b) Interpretation of Mössbauer spectra of dioctahedral Fe^{3+}-containing 2:1 layer silicates. III. Celadonite. *Kristallografiya,* **29**, 312–321 (in Russian).

Dainyak L.G., Drits V.A. & Heifits L.M. (1992) Computer simulation of cation distribution in dioctahedral 2:1 layer silicates using IR-data: Application to Mössbauer spectroscopy of a glauconite sample. *Clays Clay Miner.* **40**, 470–479.

Dainyak L.G., Bookin V.A., Drits V.A. & Tsipursky S.I. (1981) Mössbauer and electron diffraction study of cation distribution in celadonite. *Acta Cryst.* **A37 (suppl.)**, C-362.

Dainyak L.G., Dainyak B.A., Bookin A.S. & Drits V.A. (1984c) Interpretation of Mössbauer spectra of dioctahedral Fe^{3+}-containing 2:1 layer silicates. I. Computation of electric field gradients on the basis of structural modelling. *Kristallografiya*, **29**, 94–100 (in Russian).

De Grave E., Vandenbruwaene J. & Elewaut E. (1985) An ^{57}Fe Mössbauer effect study on glauconites from

different locations in Belgium and northern France. *Clay Miner.* **20,** 171-179.

Drits V.A. & McCarty D. (1996) Diffraction effects from illite and illite-smectites consisting of interstratified *trans*-vacant and *cis*-vacant 2:1 layers; a semi-quantitative technique for determination of layer-type content. *Am. Miner.* **81**, 852−863.

Drits V.A., Tsipursky S.I. & Plançon A. (1984b) Application of the method for the calculation of intensity distribution to electron diffraction structure analysis. *Izvestiya Akademii Nauk, Ser. Phys.* **2**, 1708−1713 (in Russian).

Drits V.A., Weber F., Salyn A.L. & Tsipursky S.I. (1993a) X-ray identification of one-layer illite varieties: application to the study of illites around uranium deposits of Canada. *Clays Clay Miner.* **41**, 389−398.

Drits V.A., Plançon A., Sakharov B.A., Besson G., Tsipursky S.I. & Tchoubar C. (1984a) Diffraction effects calculated for structural models of K-saturated montmorillonite containing different types of defects. *Clay Miner.* **19**, 541−562.

Drits V.A., Kameneva M.Yu., Sakharov B.A., Dainyak L.G., Tsipursky S.I., Smoliar B.B., Bookin A.S. & Salyn A.L. (1993b) *Problems of the determination of the actual crystal structures of glauconites and related minerals,* 200 pp. Novosibirsk, Nauka (in Russian).

Govaert A., De Grave E., Quartier H., Chambaere D. & Robrecht G.G. (1978) Mössbauer analysis of glauconites of different Belgian finding places. *J. Phys. Colloq.* **C2**, 442−444.

Hargraves P., Rancourt D.C. & Lalonde A.E. (1990) Single-crystal Mössbauer study of phlogopite mica. *Can. J. Phys.* **68**, 128−144.

Heller-Kallai L. & Rozenson I. (1981) The use of Mössbauer spectroscopy of iron in clay mineralogy. *Phys. Chem. Min.* **7**, 223−238.

Ivanovskaya T.A., Tsipursky S.I. & Yakovleva O.V. (1989) Mineralogy of globular glauconites from Vendian and Rephean of the Urals and Siberia. *Litologiya and poleznii iskopaemiya,* **3**, 83−89 (in Russian).

Johnston J.H. & Cardile C.M. (1987) Iron substitution in montmorillonite, illite, and glauconite by ^{57}Fe Mössbauer spectroscopy. *Clays Clay Miner.* **35**, 170−176.

Kotlicki A., Szczyrba J. & Wiewiora A. (1981) Mössbauer study of glauconites from Poland. *Clay Miner.* **16**, 221−230.

Malkova K.M. (1956) On celadonite of Pobuzhyie. *Zapiski Lvovskogo Mineralogicheskogo obchestva,* **10**, 305−318 (in Russian).

Manceau A. & Calas G. (1986) Nickel-bearing clay minerals; II. Intracrystalline distribution of nickel: an X-ray absorption study. *Clay Miner.* **21**, 341−360.

Manceau A. & Combes J.M. (1988) Structure of Mn and Fe oxides and oxyhydroxides: a topological approach by EXAFS. *Phys. Chem. Min.* **15**, 283−295.

Manceau A., Bonnin D., Stone W.E.E. & Sanz J. (1990) Distribution of Fe in the octahedral sheet of trioctahedral micas by polarized EXAFS. Comparison with NMR results. *Phys. Chem. Min.* **17**, 363−370.

Murad E. & Wagner U. (1994) The Mössbauer spectrum of illites. *Clay Miner.* **29**, 1−10.

McKale A.G., Veal B.W., Paulikas A.P., Chan Sk. & Knapp G.S. (1988) Improved *ab initio* calculations of amplitude and phase functions for extended X-ray absorption fine structure spectroscopy. *J. Am. Chem. Soc.* **110 12**, 3763−3768.

Pavlishin V.I., Platonov A.N., Polshin E.V., Semenova T.F. & Starova G.K. (1978) Micas with iron in tetrahedral coordination. *Zapiski Vsesouznogo Mineralogicheskogo obchestva*, **107**, 165−175 (in Russian).

Popov V.I., Khramov D.A. & Lobanov F.I. (1988) Absorber shape: The influence on the Mössbauer specrum parameter. *Proc. USSR Conf. Appl. Mössbauer Spectroscopy "Volga", Moscow*, 32−33 (in Russian).

Rancourt D.G. (1994) Mössbauer Spectroscopy of Minerals. II Problem of resolving cis and trans octahedral Fe^{2+} sites. *Phys. Chem. Min.* **21**, 250−257.

Reynolds R.C. & Thompson C.H. (1993) Illite from the Potsdam Sandstone of New York, a probable noncentrosymmetric mica structure. *Clays Clay Miner.* **41**, 66−72.

Rozenson I. & Heller-Kallai L. (1978) Mössbauer spectra of glauconites reexamined. *Clays Clays Minerals* **26**, 173−175.

Sainctavit Ph., Petiau J., Manceau A., Rivallant R., Belakhovsky M. & Renaud G. (1988) A two-mirror device for higher harmonic rejection. *Nucl. Instrum. Methods,* **A 273**, 423−428.

Sakharov B.A., Besson G., Drits V.A., Kamaneva M.Y., Salyn A.L. & Smolyar B.B. (1990) X-ray study of the nature of stacking faults in the structure of glauconites. *Clay Miner.* **25**, 419−435.

Shutov V.D., Drits V.A., Kats M. Ya. & Sokolova A.L. (1975) Crystal chemistry of glauconites as indicator of facial conditions of formation and postsedimentary transformation of these minerals. Pp. 74−81 in: *Crystal Chemistry of Minerals and Geological Problems* (A.G. Kossovskaya, editor). Nauka, Moscow (in Russian).

Slonimskaya M.V., Besson G., Dainyak L.G., Tchoubar C. & Drits V.A. (1986) The interpretation of the IR spectra of celadonites and glauconites in the region of OH stretching frequencies. *Clay Miner.* **21**, 377−388.

Smoliar-Zviagina B.B. (1993) Relationships between structural parameters and chemical composition of

micas. *Clay Miner*. **28**, 603–624.

Teo B.K (1986) *EXAFS: Basic Principles and Data Analysis*, *Inorg. Chem. Concepts,* Springer Verlag, New York.

Townsend M.G., Longworth G., Ross C.A. & Provenchez R. (1987) Ferromagnetic or antiferromagnetic Fe III spin configurations in sheet silicates. *Phys. Chem. Min.* **15**, 64–70.

Tsipursky S.I. & Drits V.A. (1984) The distribution of octahedral cations in the 2:1 layers of dioctahedral smectites. *Clay Miner.* **19**, 177–193.

Tsipursky S.I., Drits V.A. & Chekin S.S. (1978) Study of structural ordering of nontronite by oblique texture electron diffraction. *Izvestiya Akademii Nauk S.S.S.R., Ser. Geol.* **10**, 105–113 (in Russian).

Tsipursky S.I., Drits V.A. & Plançon A. (1985) Calculation of the intensities distribution in oblique texture electron diffraction patterns. *Kristallografiya*, **30**, 38–44 (in Russian).

Zvyagin B.B., Rabotnov V.T., Sidorenko O.V. & Kotelnikov D.D. (1985) Unique mica consisting of noncentrosymmetric layers: *Izvestiya Akademii Nauk S.S.S.R., Ser. Geol.* **35**, 121–124 (in Russian).